TÉCNICO LISBOA

Energetic Analysis of the Ankle Musculoskeletal Complex with a Passive Spring Exoskeleton

Maria Leonor Palminha Alves

Thesis to obtain the Master of Science Degree in

Biomedical Engineering

Supervisors: Prof. Jorge Manuel Mateus Martins
Maj MAT Luís Filipe Pratas Quinto

Examination Committee

Chairperson: Prof. João Orlando Marques Gameiro Folgado
Supervisor: Prof. Jorge Manuel Mateus Martins
Member of the Committee: Rui Miguel de Moura Antunes e Valejo Coelho, PhD

November 2021

Declaration

I declare that this document is an original work of my own authorship and that it fulfills all the requirements of the Code of Conduct and Good Practices of the Universidade de Lisboa.

Preface

The work presented in this thesis was performed at the IDMEC - Instituto de Engenharia Mecânica of Instituto Superior Técnico (Lisbon, Portugal), during the period March-October 2021, under the supervision of Prof. Jorge Martins. The thesis was co-supervised at the Military Academy by Maj. Luís Quinto.

Acknowledgments

First of all I would like to thank Professor Jorge Martins, Professor Miguel Tavares da Silva and Major Luís Quinto for all their help and guidance throughout this work. I'd also like to thank Pawel Bujalski for sharing his expertise and providing me with the data he collected for his dissertation.

The author would like to thank the Portuguese Army, through CINAMIL, within project ELITE2 - Enhancement LITe Exoskeleton, for supporting this research.

I'd like to thank my parents and my grandma for their support and encouragement. A word of thanks to all my friends who kept me sane throughout this pandemic, through online hangouts and movie nights. A special thanks to my cousin who proofread this dissertation and provided mutual understanding and support.

Resumo

O melhoramento das capacidades físicas humanas tem estado na vanguarda do desenvolvimento de exoesqueletos na última década. Nomeadamente, dispositivos passivos estão a ser desenvolvidos e estudados com o intuito de reduzir o custo metabólico da marcha. Nesta dissertação apresenta-se um modelo computacional do complexo musculoesquelético do tornozelo com o objectivo de estudar a mecânica e energética desta articulação durante o ciclo da marcha, quer quando auxiliada por um dispositivo quer não.

O modelo desenvolvido é composto pelo soleus e tibialis anterior, bem como uma mola de rigidez linear em paralelo com a articulação, que lhe acrescenta momento durante a fase de apoio. Cada músculo é modelado através de um modelo tipo Hill acoplado a um modelo muscular de gasto energético, o que permite a análise simultânea de alterações na mecânica e energética dos músculos durante a variação da rigidez da mola entre 0 de 200 Nm/rad. É também analisado o custo metabólico total associado à articulação, para o qual é obtido um mínimo para uma rigidez intermédia de 150 Nm/rad. Este resultado suporta a possibilidade de reduzir o custo metabólico da marcha através de dispositivos passivos. Simultaneamente, o mesmo resultado evidencia que alterar o ciclo de marcha natural, sem uma análise cuidada, pode levar a um aumento do custo metabólico durante o ciclo de marcha.

Palavras-chave: Biomecânica, Modelação musculoesquelética, Marcha, Custo metabólico, Exoesqueleto passivo.

Abstract

The augmentation of human capabilities has been at the forefront of exoskeleton development in the past decade. Recently, passive devices have been developed and studied as an option for reducing the metabolic cost during gait. In this dissertation, a computational model of the ankle musculoskeletal complex is developed with the intention of studying the mechanics and energetics of this joint during the gait cycle, whether aided by an exoskeleton or not.

The developed model is composed of the soleus and the tibialis anterior, as well as a linear stiffness spring in parallel with the joint, which provides an added moment during stance. Each muscle is modeled as a Hill-type muscle coupled to an energy expenditure muscle model. This allows for the simultaneous analysis of changes to both mechanics and energetics of the muscles when spring stiffness is varied between 0 and 200 Nm/rad. The total metabolic cost associated with the joint is also analysed and a minimum is reached for an intermediate stiffness of 150 Nm/rad. This finding supports the idea of reducing the metabolic cost of walking using passive devices, while providing evidence that altering the natural gait cycle, without careful analysis, can lead to an increase in its metabolic cost.

Keywords: Biomechanics, Musculoskeletal modelling, Gait, Metabolic cost, Passive exoskeleton

Contents

List of Tables

List of Figures

Glossary

ADLs Activities of Daily Living.

BE Buffer Element.

CE Contractile Element.

EDT Emerging and Disruptive Technology.

EMG Eletromyography.

FF Foot Flat.

FS Forefoot Strike.

FT Fast Twitch.

HR Heel Rise.

HS Heel Strike.

IC Initial Contact.

MTU Muscle Tendon Unit.

NASA National Aeronautics and Space Administration.

NATO North Atlantic Treaty Organization.

PCSA Physiological Cross-Sectional Area.

PE Contractile Element.

PO push off.

SCI Spinal Cord Injury.

SE Series Element.

ST Slow Twitch.

TA Tibialis Anterior.

TO Toe Off.

TV Tibia Vertical.

Chapter 1

Introduction

1.1 Motivation

Walking is the most common of human movements and, although it is one of the most complex completely integrated movements, it is one that has been perfected throughout the centuries [1]. When walking, humans keep energy expenditure to a minimum, by for example adjusting their step length and arm motion. Despite this natural tendency towards minimizing energy costs during walking, humans still spend an overwhelming amount of energy on this activity, especially in demanding conditions [2].

Developing and studying strategies to further reduce this cost could, therefore, prove useful in many settings. Not only by effectively reducing the metabolic cost of walking, and thus allowing individuals to walk farther or carry more weight, but also by reducing fatigue, increasing mobility and reducing the risk of injury [2, 3].

The reduction of the metabolic cost of walking is the goal of many exoskeleton technologies being developed [4]. One of the most promising exoskeletons developed with this purpose is the ankle exoskeleton developed by Collins et al. [2]. While most of these solutions are active, this one is passive, that is, it relies solely on passive elements, a spring for actuation, making it lighter. Recently, a prototype inspired by that of Collins et al. was developed at IST by Machado [5]. This ankle exoskeleton is quasi-passive, meaning that, while relying on passive elements for actuation it makes use of electronic components for controlling said actuation system.

In order to further develop these technologies, a deeper understanding of the mechanisms underlying the mechanics and energetics of the ankle during gait, both aided and unaided, is required. This work focuses on developing a computational model for studying the ankle complex muscles' mechanics and energetics when a linear stiffness spring is added to the joint and analysing the potential decrease in metabolic cost.

1.2 Objectives

The main goal of this work is to study the effect of an ankle exoskeleton on the ankle joint's muscle mechanics and consequently energy expenditure. This is achieved through the development of a computational model of the ankle musculoskeletal complex which integrates, for each muscle studied, a muscle tendon model with an energy expenditure model, coupled with a spring.

Thus, the goals of this project are:

- Implementation of the energy expenditure model.
- The development of the ankle musculoskeletal complex computational model.
- Application of the developed model to locomotion data.
- Analysis of the effect of the exoskeleton on the energy expenditure during locomotion, based on the results from the previous goal.

1.3 Contributions

The work developed for this dissertation contributes to further the understanding of the energy expenditure of locomotion both aided by a passive device and unaided, through the development of a musculoskeletal energy expenditure model of the ankle complex. This work also contributes with further evidence that a spring actuated exoskeleton can provide a meaningful reduction of the energy expended during locomotion, and uncovers the bounding conditions under which this reduction occurs.

1.4 Thesis Outline

This dissertation is composed of 6 chapters. Chapter 2 is introductory and covers the theoretical background of this work, as well as the state-of-the-art. Chapter 3 describes the muscle models used in this dissertation. Chapter 4 describes the problem at hand and the steps taken to achieve a solution. In chapter 5, the obtained results are analysed and discussed. The last chapter is reserved for the conclusions along with suggestions for future research.

Chapter 2

Background

2.1 Biomechanics

Biomechanics is the study of biological systems using the laws of mechanics, most often that biological system is the human body. Mechanics is the branch of physics which analyses the motion of a particular system and the effect of forces on said system. The analysis of human motion requires specific terminology to accurately describe postures and motions. Anatomy, the study of the structure of the human body, provides the terminology required for biomechanical analysis [6].

2.1.1 Key Anatomical Concepts

Anatomy describes the human body and its motions relative to the anatomical reference position. This position, shown in figure 2.1, corresponds to the upright position with the feet slightly apart and the arms suspended sideways, with the palms facing forward. A plane of motion is a spatial direction in which motion occurs and an axis is an imaginary line about which the body rotates [6]. The human body is transected by three imaginary orthogonal planes, which divide the body in halves:

- Sagittal Plane - orthogonal to the sagittal axis while containing the frontal and transverse axes, it separates the body in left and right. Structures closer to the midline of the body are medial or interior, while those further are lateral or exterior [7].
- Frontal Plane - orthogonal to the frontal axis while containing the sagittal and transverse axes, it separates the body in anterior and posterior. Structures towards the back of the body are posterior, while structures towards the front of the body are anterior [7].
- Transverse Plane - orthogonal to the transverse axis while containing the sagittal and frontal axes, it separates the body in superior and inferior. Structures higher up in the body are superior, while those lower in the body are inferior [7].

When the body is in the anatomical reference position, all anatomical segments are considered at the origin, when describing relative orientations. Rotation of an anatomical segment with respect to another

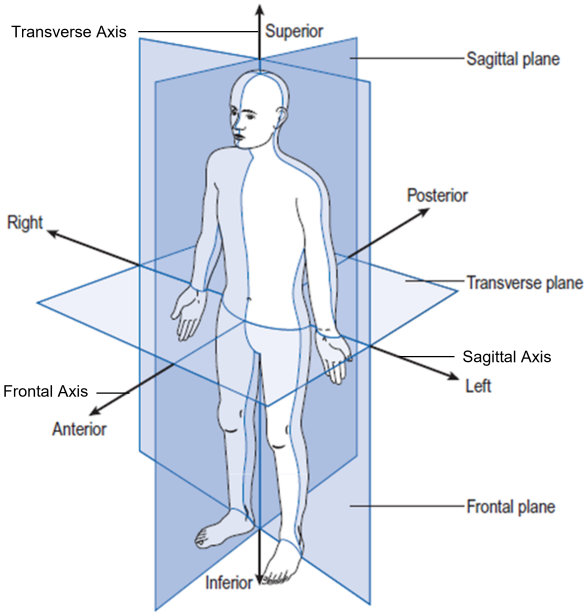

Figure 2.1: Human body in the anatomical reference position with the three reference planes and axis. Adapted from Whittle [7].

is referred according to the direction of motion and measured as the angle between the current position and the anatomical position [8]. Simple motions can be split according to the plane in which they take place:

- Sagittal Plane Movements
  - Primary Movements
    - Flexion - movement that decreases the angle between two anatomical segments.
    - Extension - movement that returns the anatomical segment to the anatomical position.
    - Hyperextension - rotation beyond the anatomical reference position in the direction opposite flexion.
  - Foot Movement
    - Dorsiflexion - movement that brings the foot towards the lower leg.
    - Plantar flexion - movement that moves the foot away from the lower leg.

- Frontal Plane Movements
  - Primary Movements
    - Abduction - movement of the body segment away from the midline of the body.
    - Adduction - movement of the body segment towards the midline of the body.
  - Foot Movement
    - Eversion - outward rotation of the sole of the foot .
    - Inversion - inward rotation of the sole of the foot.

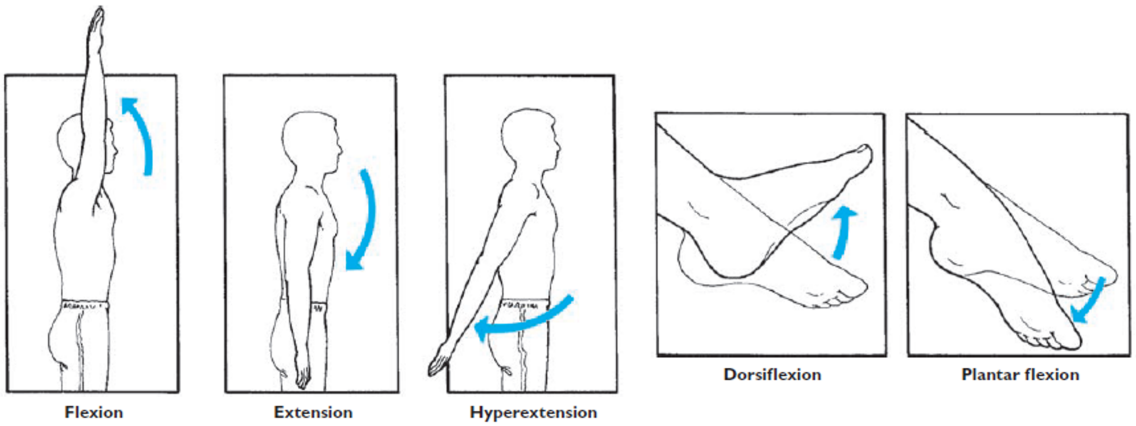

Figure 2.2: Movements in the sagittal plane [8].

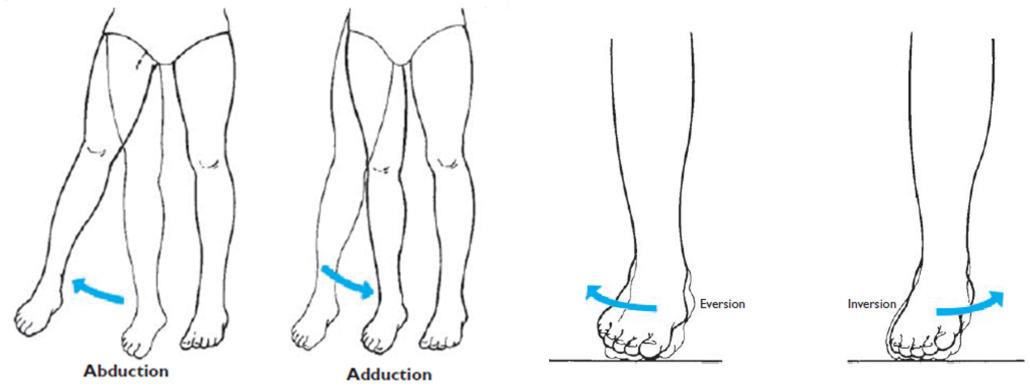

Figure 2.3: Movements in the frontal plane. Adapted from Hall [8].

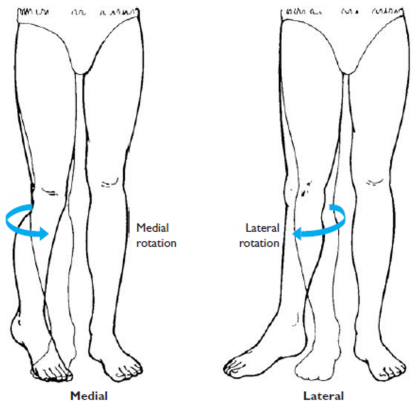

Figure 2.4: Movements in the transverse plane [8].

- Transverse Plane Movements
  - Primary Movements
    - Medial Rotation - rotation towards the midline of the body.
    - Lateral Rotation - rotation away from the midline of the body.

2.1.2 Skeletal Muscle

The muscle is an excitable tissue, capable of actively generating contractile force. The main function of skeletal muscle is to generate and transmit force to the bones, this is achieved by generating moments of force that act on the joints crossed by the muscle. The four main properties of the muscle tissue are extensibility, elasticity, irritability and contractility [8].

Extensibility is the ability to increase in length, while contractility is the ability to decrease in length. Elasticity is the tissue's capacity of returning to its resting length following lengthening or contraction. The muscle is a viscoelastic tissue, meaning that its elasticity profile is time dependent. The elastic behavior of the muscle is associated with the connective tissue that makes up the muscle membranes that surround the muscle fibers, as well as with the tendon. Irritability is the muscle's ability to respond actively to a stimulus, whether internal, at the neuromuscular junction, or external [8].

The structural unit of the muscle is the sarcomere (Figure 2.5B,C), which is composed of two bands: one thicker and containing myosin filaments (A band), the other thinner and containing actin filaments (I band). These protein filaments are attached at the Z lines, which are connected to the surrounding membrane, the sarcolemma. Muscle contractions are initiated when muscle fibers are stimulated by a nervous impulse. Calcium ions (Ca^{2+}) are released from the sarcoplasmatic reticulum, allowing the myosin filaments to bind to the actin filaments, in what is called the cross-bridge cycle [7]. Sarcomeres are organized in myofibrils and a muscle fiber (or cell), figure 2.5A, is composed of several myofibrils.

Skeletal muscle fibers are divided, based on the time it takes them to reach maximum tension after being stimulated, into two categories: Slow Twitch (ST) and Fast Twitch (FT) fibers. Slow twitch fibers are smaller than fast twitch fibers and are also more capillarized and have a larger number of mitochondria. Thus, slow twitch fibers have a higher capacity for aerobic metabolism, while fast twitch fibers rely mostly on anaerobic pathways [9]. Most skeletal muscles contain both types of fibers, with their proportion varying depending on the muscle.

When the muscle produces a torque larger than the resistive torque at the joint it actuates, a concentric contraction (figure 2.6a) occurs, and the muscle shortens resulting in a movement in the same direction as the net torque generated by the muscle. An eccentric contraction (figure 2.6b) occurs when the opposing torque at the joint exceeds the one produced by the muscle and the muscle lengthens, resulting in a movement opposite the muscle's torque. When the resistive torque is equal to that produced by the muscle, it does not shorten or lengthen and no movement occurs at the joint. In this case the contraction is isometric (figure 2.6c) [8].

The performance of movements generally involves the cooperative action of several muscle groups. Muscles that generate movement when contracting are called agonists. Moreover, a distinction can

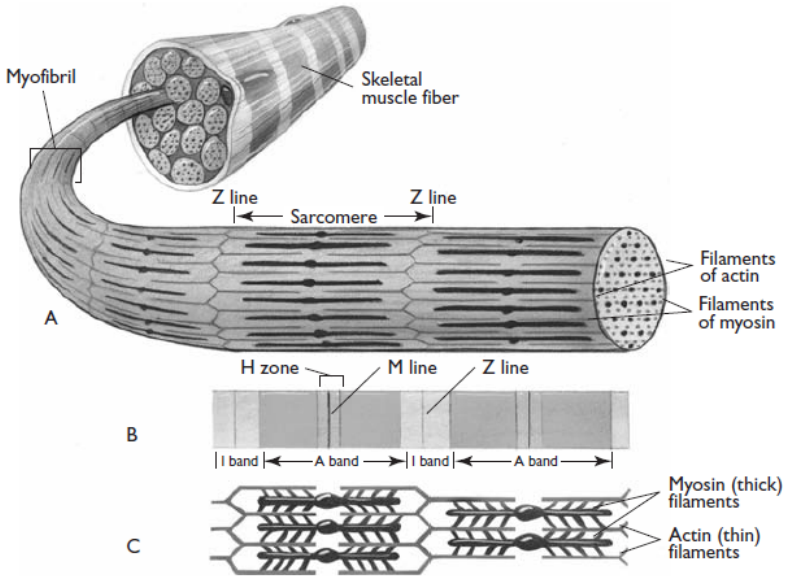

Figure 2.5: Skeletal muscle fiber representation [8].

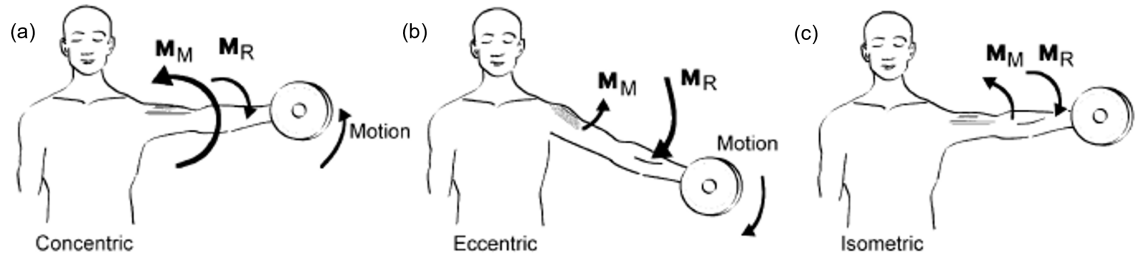

Figure 2.6: Three types of muscle contraction: concentric, eccentric and isometric. M_R and M_M are the resistive and muscle torques, respectively. Adapted from Knudson [6].

be made between primary and assistant agonists when more than one muscle acts in the movement. The muscles that oppose the movement are called antagonists. These muscles contract eccentrically as the agonists develop concentric contractions. Typically antagonists act as a brake during movement. Stabilizers are muscles that aid in stabilizing a body part against a given force, while neutralizers prevent certain unwanted actions that occur when agonist muscles act [8].

2.2 Human Gait

Gait is the most common of human movements and its sole purpose is to transport the body across the ground, whether that be by walking or running [1]. Since gait is a repetitive motion, it is often analysed as a cycle. The gait cycle "is defined as the time interval between two successive occurrences of one of the repetitive events" of the motion [7]. The most usual occurrence chosen for this purpose is the Initial Contact (IC) of one of the feet. The event between the IC of a foot and the IC of the same foot is a stride, while the event between the IC of one foot and that of the contralateral foot is a step [1].

The performance of the gait cycle relies on certain functions that the human body must achieve. It must generate mechanical energy in order to propel the body forward, but also absorb mechanical energy for stability and shock absorption. Maintenance of an upright posture and upper body support are also necessary, and the foot trajectory must be controlled [1]. While there is movement in all anatomical reference planes, most of the relevant movement during gait occurs in the sagittal plane [10].

The gait cycle is divided in two phases: the stance phase, when the foot is in contact with the ground, and the swing phase, when the foot is no longer in contact with the ground. The stance phase makes up 60% of the cycle while the swing phase corresponds to the remaining 40%. However, as speed increases, the stance phase is shortened [7]. Each of these phases is further divided into smaller periods.

The stance phase is subdivided into four periods. The loading response is comprised between Initial Contact (IC) and Toe Off (TO) of the contralateral foot, which more or less coincides with Foot Flat (FF). During this period of double support, the body weight is being shifted to the forward limb. In non-pathological walking, Initial Contact is made with the heel (Heel Strike (HS)), while for running it is usually done with the forefoot (Forefoot Strike (FS)). During single limb support, it is possible to identify two periods: mid-stance, from FF to Heel Rise (HR), and terminal stance, from HR to IC of the contralateral limb. Next follows pre-swing, another period of double limb support, during which the body weight is being transferred to the opposite limb, ending at Toe Off [7, 11]. Push off (PO), comprised between HR and TO, is the period in which powered plantar flexion occurs, pushing the lower limb away from the ground [1].

The swing phase is divided into three periods. Initial swing starts at TO and ends when the feet are adjacent. Mid-swing follows, terminating when the tibia of the swinging foot is vertical. Terminal swing initiates with Tibia Vertical (TV) and ends with IC. A new stride begins, continuing the cycle [7]. Figures 2.7 and 2.8 illustrate the gait cycle and its phases.

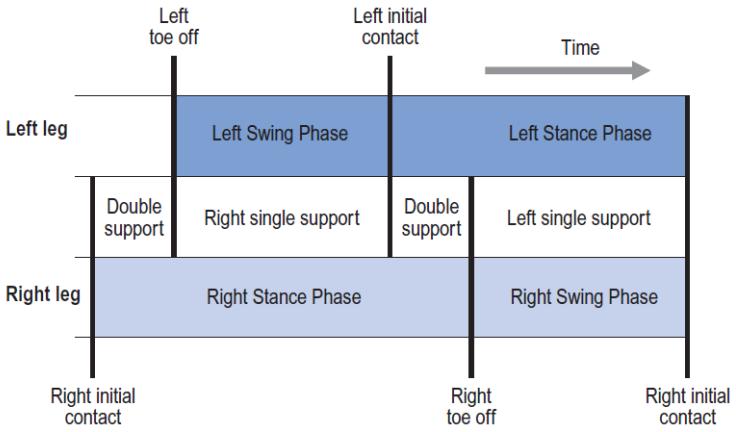

Figure 2.7: Representation of the gait cycle starting with the right leg's initial contact and illustrating the moments of double and single limb support. Adapted from Whittle [7].

Human gait "involves the integrated activity of muscles acting across many joints" [1], therefore, there is a certain redundancy in the movement. In other words, the same movement can be achieved through different combinations of muscle activation. That is why the analysis of the kinematics and dynamics

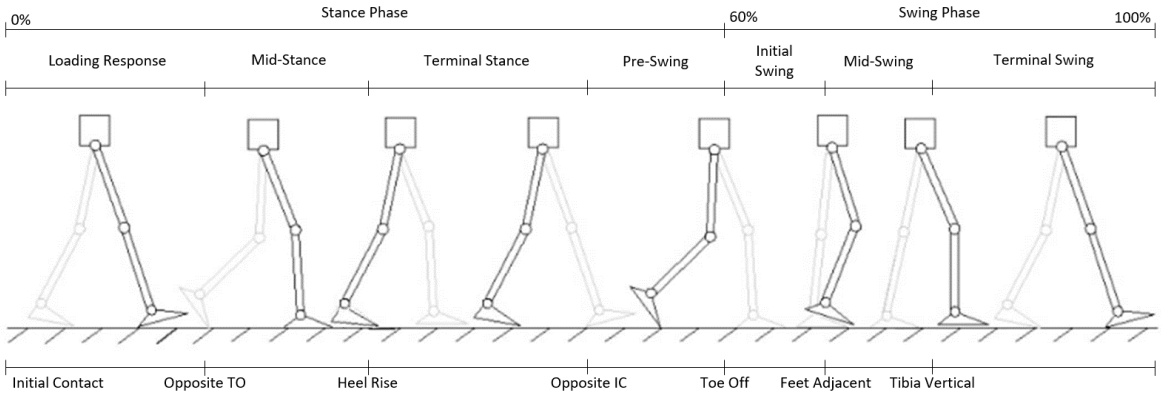

Figure 2.8: Representation of the gait cycle starting with the right leg's initial contact and illustrating its different phases and periods. Adapted from Dollar and Herr [12].

of gait provide crucial information on the gait cycle. Kinematics is the area of study of the motion without considering the forces involved. It "describes the motion in terms of displacement, velocity and acceleration in space" and the "relative motion between rigid bodies" [10], while dynamics takes into account the effects of forces and torques on the rigid bodies. Since the overall gait pattern is similar, both intra- and inter-subject, it is possible to analyse gait data according to normalized universal patterns [1]. This analysis tends to focus on certain well studied variables, such as joint angles, moments and power, as these provide a good understanding of the underlying mechanisms [7]. The reference curves for these variables are presented in figure 2.9.

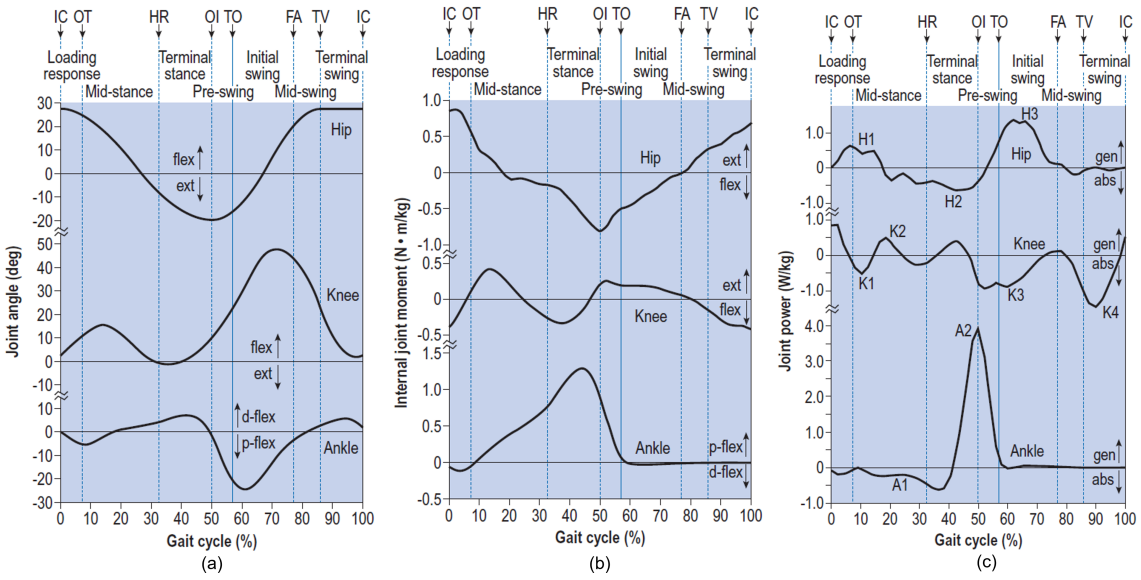

Figure 2.9: Variation along the gait cycle in the sagittal plane of: (a) joint angles; (b) joint moments; (c) joint power. Where IC - initial contact; OT - opposite toe off; HR - heel rise; OI - opposite initial contact; TO - toe off; FA - feet adjacent; TV - tibia vertical; H1, H3 - hip's power generation peaks; H2 - hip's power absorption peak; K1, K3, K4 - knee's power absorption peaks; K2 - knee's power generation peak; A1 - ankle's power absorption peak; A2 - ankle's power generation peak [7].

2.2.1 Ankle Gait Dynamics

From the reference curve for joint power (figure 2.9c), it is clear that the ankle is the joint that produces highest peak power during the gait cycle, namely during push off. In addition to this, it is estimated that the plantarflexors expend approximately 27% of the metabolic energy used for walking [2]. Therefore, a reduction in the metabolic cost of gait should inherently be focused on the ankle. A detailed account of the ankle's kinematics and dynamics during each phase of the gait cycle are presented below.

The ankle joint is composed by the distal tibiofibular, tibiotalar and fibulotalar joints. Most ankle motions occur at the tibiotalar joint, which is primarily a hinge joint. During gait, ankle motions occur mostly in the sagittal plane. Therefore, muscles can be classified, based on their function, into plantarflexors and dorsiflexors (figure 2.10). Plantarflexors are active during stance, while the dorsiflexors are active during loading response and swing. Four muscles, anterior to the ankle, can be considered dorsiflexors: Tibialis Anterior (TA), extensor digitorum longus, extensor hallucis longus and peroneus tertius [8, 11]. A muscle's capacity to generate moment is dependent both on their cross-sectional area and their lever arm. Even though these muscles have similar lever arms, the TA has the largest cross-sectional area, hence it is the most important muscle for dorsiflexion. Seven muscles, posterior to the ankle, can be considered plantarflexors. The soleus and gastrocnemius, collectively known as triceps surae, are the main plantarflexors. The assistant plantarflexors are grouped in the perimalleolar functional group [8, 11].

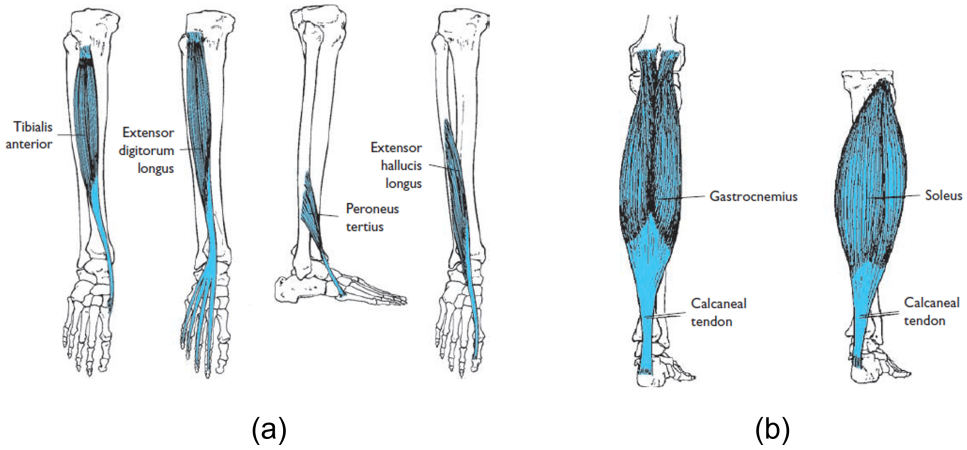

Figure 2.10: Major muscles acting on the ankle joint: (a) dorsiflexors; (b) plantarflexors [8].

During the gait cycle the ankle performs four arcs of motion, intercalating between plantarflexion and dorsiflexion (figure 2.9a), while "none of these motions are large, they are critical for progression and shock absorption [11]."

- The first arc of motion is triggered by Initial Contact. At this time the ankle is close to its neutral position, either in dorsi- or plantarflexion. When the heel strikes the floor there is a fast plantarflexion motion, the Tibialis Anterior is active and contracting eccentrically, generating a small dorsiflexor moment and absorbing power, in order to control the lowering of the foot to the floor [7, 11].
- After FF occurs dorsiflexion begins, as the tibia moves over the stationary foot. At this point the

TA stops contracting, while the soleus and then the gastrocnemius, begin contracting eccentrically, absorbing power and generating considerable plantar flexion moment, as well as allowing the Achilles tendon to stretch and store energy. Both dorsiflexion angle and plantar flexion moment peak during terminal stance [7].

- The move into plantar flexion occurs late in terminal stance, when the triceps surae begin contracting concentrically. When the opposite limb contacts the floor the weight is quickly transferred, releasing the tension on the triceps surae, this allows the stretched tendon to recoil which, coupled with concentric contraction, results in the highest generation of power of the cycle. This peak in power corresponds to the push off, which propels the limb into the swing phase. The peak of plantar flexion occurs right after toe off, although triceps surae contraction ends before this event, as evident by the decrease in power generation at the joint [7, 11].

- The Tibialis Anterior begins to contract in order to return the ankle to a neutral or dorsi-flexed position to ensure the foot clears the floor during swing. Once the toes have cleared the floor the position of the ankle is kept more or less neutral. The TA continues to contract and its activity increases prior to IC [7].

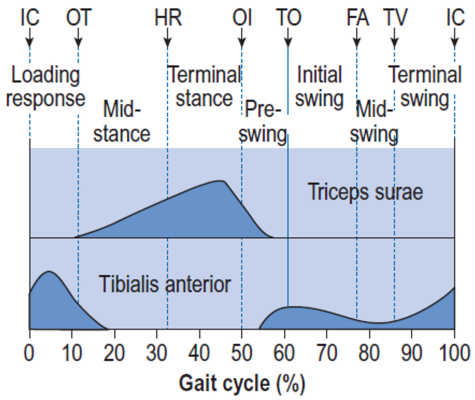

Figure 2.11: Activation profile of the triceps surae (gastrocnemius and soleus) and tibialis anterior during the gait cycle. Adapted from Whittle [7].

2.2.2 Energetics of Gait

Most of the energy expended by individuals during the day goes towards walking, even though the human body has evolved to walk in a manner that reduces the energy consumed [2, 10]. Metabolic energy, which comes from ingested and stored nutrients, is required for muscle contraction and relaxation. Therefore, the metabolic cost of walking "is set by muscles that act to perform work on the center of mass, swing the legs relative to the center of mass, and support body weight [13]."

Measuring the metabolic cost of human activities provides insight into their demand on the body. The analysis and comparison of these measurements, for different activities or for the same activity performed under different conditions, can help find ways to reduce energy expenditure or quantify the

benefit provided by an external device, such as an ankle exoskeleton. In a laboratory setting, metabolic cost can be measured through direct or indirect calorimetry. Direct calorimetry measures the body's heat and work production. However, it requires large and expensive devices, so indirect calorimetry is most often used in practical settings. This second method estimates energy expenditure based on respiratory gas exchange measurements, that is, a spirometer is used to measure the amount of carbon dioxide expired and the amount of oxygen inspired, and thus compute the oxygen uptake (VO_2) [14].

Calorimetry methods only provide a whole body estimate of energy expenditure, when often the expenditure of single muscles or joints is of greater interest. In light of this limitation, many researchers have developed energy expenditure models which use variables acquired during movement analysis, such as muscle forces, lengths and activations, in order to estimate the energy expended by a given muscle [15]. The developed models can be Huxley-based, which provide a link between force production and crossbridge thermodynamics, but do not fare well for large-scale simulations, or Hill-based, which are most often used. Hill-based models differ on the data their parameters derive from, but also in the way they take into account eccentric work [16].

One Hill-based model of great interest and which has been employed by many researchers, is that developed by Umberger et al. [17], which will be detailed in section 3.2. In addition to providing average muscle specific energy expenditure, this model also "allows the time profile of the metabolic rate to be computed", therefore providing information on metabolic consumption throughout the movement [18].

2.3 Exoskeletons and Locomotion Aids

Herr [19] defines robotic exoskeletons as "mechanical devices that are anthropomorphic in nature, are 'worn' by an operator and fit closely to the body, and work in concert with the operator's movements." Exoskeletons can be divided into three broad categories according to their purpose: human performance augmentation, assistive devices for disabled individuals and therapeutic exoskeletons for rehabilitation [3, 20].

Human performance augmentation exoskeletons have as their ultimate goal to augment the strength, endurance or any other capability of an able bodied individual. These exoskeletons show promising uses in industrial, military and civilian settings. Assistive exoskeletons for individuals with disabilities encompass various types of exoskeletons whose aim is to allow individuals impaired by, for example a stroke or a Spinal Cord Injury (SCI), to perform movements which they are not able to complete by themselves [20]. Rehabilitation exoskeletons are tools used by physical therapists to provide intense repetitive motions to the patients' limbs, thus improving their musculoskeletal strength and motor control, minimizing the functional deficits caused by their disability [3].

Research and development regarding exoskeletons has increased exponentially in the past decade as technology evolved. According to de la Tejera et al. [21], from 2010 to 2015 there were 3147 publications regarding this technology, while from 2016 to 2020 this number increased to 5244, showing the clear tendency for growth in the area. NATO has also identified exoskeletons as an Emerging and Disruptive Technology (EDT) in the Biotechnology and Human Enhancement field [22].

2.3.1 Classification

In addition to the categories mentioned above, exoskeletons may be categorized according to several different aspects. Regarding structure, exoskeletons may be soft (Figure 2.13c), or rigid and may work in series or in parallel with the user [19, 21]. Furthermore, exoskeletons may be designed for the full body, upper body, lower body, or even for specific limbs or joints [21]. Due to the scope of this work, the focus will be on lower limb exoskeletons. A distinction can also be made as to the type of action they possess:

Active Exoskeleton

The energy needed to perform the movement is supplied by external sources. These devices rely on electric, hydraulic or pneumatic actuators and power sources to produce movement [21] and are used as assistive devices for disabled individuals, since these users would not be able to produce the movement autonomously [20].

Passive Exoskeleton

The user performs the movement with the aid of the exoskeleton. These devices typically make use of mechanical systems which store and transmit energy and are mostly used for human performance augmentation purposes [21].

Quasi-passive Exoskeleton

Quasi-passive exoskeletons use passive mechanical systems, but are equipped with electronic sensors allowing for the control of said systems.

Another important aspect of exoskeleton classification is their area of application. Exoskeletons may be used in the following fields:

Military

Exoskeletons used in any branch of the armed forces - the goal is to reduce metabolic cost of movement and help in carrying loads during missions, as well as avoiding injuries[21, 23].

Clinical

Encompasses both assistive devices for disabled individuals and therapeutic exoskeletons for rehabilitation.

Industrial

Exoskeletons used by healthy individuals to avoid injuries caused by repetitive motions or heavy load carrying [21].

Civilian

Exoskeletons for general population use. For example for elderly individuals, in order to aid in performing Activities of Daily Living (ADLs) [21, 24], or in civilian operations for use by first responders during search and rescue missions or firefighting [20].

2.3.2 Current Solutions

As stated before the interest in exoskeleton technology has been rising, with both companies and research teams developing prototypes and commercially available exoskeletons. This section will provide detail on examples of said devices.

Human Performance Augmentation

Performance augmentation exoskeletons can be built with different goals in mind. For example: load bearing, metabolic cost reduction or to provide support during repetitive and prolonged motions.

BLEEX (figure 2.12a) was the first untethered, that is, energetically autonomous, lower limb exoskeleton to be able to carry a payload [25]. Through its frame, the exoskeleton transfers both its weight and that of a backpack to the ground. Furthermore the exoskeleton is guided by the user's movements instead of prescribing them, allowing for a more natural usage [20]. The ONYX exoskeleton (figure 2.12b) was developed by Lockheed Martin with the goal of reducing the metabolic cost of transport and fatigue, thereby enhancing the user's strength and endurance and helping to prevent injuries [26]. While ONYX was developed for use in a military setting, the company also produces them for first responders, and developed the FORTIS exoskeleton for industrial settings.

LegX (figure 2.12c) is a passive lower limb exoskeleton developed by SuitX, a company specializing in industrial workplace exoskeletons. Prolonged kneeling and squatting, common positions in industrial activities, such as electrical panel work and concrete laying, can increase the risk of knee injuries. LegX reduces strain on the knee by providing two working modes, a spring assisted mode and a locked mode. In spring assisted mode, the energy stored while the user squats is then released when they return to the upright position, while in the locked mode the exoskeleton supports the body weight while the user squats [27].

(a) (b) (c)

Figure 2.12: Performance Augmentation Exoskeletons: (a) BLEEX [21]; (b) ONYX [26]; (c) LegX - adapted from Pillai et al. [27]

Assistive Devices

The development of exoskeletons as assistive devices for individuals with impairments is well established. ReWalk (figure 2.13a) is currently on the market and is designed for everyday use by individuals with spinal cord injuries. Rewalk is motor actuated at the hip and knee joints, while the ankle joint is made up of a double action orthotic with spring assisted dorsiflexion. Its batteries and control system are kept in a backpack and the gait cycle is activated by tilting the torso forward, triggering the first step [28]. HAL-5 (figure 2.13b) comes in several formats: full-body and uni or bi-lateral lower-body. It stands out for its use of remaining surface Eletromyography (EMG) for controlling the exoskeleton. This makes it more suitable for patients with incomplete SCI, stroke or other similar impairments, in which the patient still has some motor function left [20].

While most research focuses on rigid frame exoskeletons some prototypes for soft solutions are being developed, such as XoSoft (figure 2.13c). This device is aimed at people with mild to moderate gait impairments, that is, stroke and incomplete SCI patients, but also elderly people. The choice of a soft structure stemmed from a multitude of reasons: it is more comfortable, easier to use independently by people with impairments and compatible with regular footwear and clothes [29].

(a) (b) (c)

Figure 2.13: Assistive Exoskeletons: (a) ReWalk [30]; (b) HAL-5 [20]; (c) XoSoft [29].

Rehabilitation Devices

Gait is one of the ADLs most affected in stroke patients and so providing adequate rehabilitation is essential to their quality of life. The H2 exoskeleton (figure 2.14a) has six actuated joints, which are controlled by an algorithm that allows torque to be applied only when the patient deviates from the normal movement pattern. This allows the patient to maintain their control, aiding them only when required [31]. The EKSO (figure 2.14b), which is bilaterally actuated at the hips and knees, is used in gait rehabilitation for patients with SCI [20]. This process is crucial both for people with incomplete injuries, who may regain the ability to walk, but also for those with complete injuries as it prevents muscle atrophy and bone density degradation.

While most rehabilitation exoskeletons are directed towards the medical market, they may be used for different applications. NASA is researching the application of the X1 (figure 2.14c), initially designed as a mobility device, as an in-space countermeasure for muscle mass and bone density degradation and as a dynamometry device [32]. The exoskeleton, which is currently actuated at the hips and knees, can provide resistance to the user's movement allowing them to perform both concentric and eccentric exercises. The data collected by the on-board sensors could then be analysed by physiologists to assess the user's progress when compared to pre-flight assessments.

(a) (b) (c)

Figure 2.14: Rehabilitation Exoskeletons: (a) H2 [31]; (b) EKSO [20]; (c) X1 [32].

2.3.3 Assistive Devices for Metabolic Cost Reduction

Recently, researchers have been focusing on ankle exoskeletons to reduce the total metabolic cost of walking. For example, the team lead by Collins [2] developed a passive exoskeleton (figure 2.15a) and an active, tethered, exoskeleton (figure 2.15b), the latter allowing both torque and work to be provided to the ankle [2, 33]. On the other hand, Mooney et al. [4] developed an active, battery powered, exoskeleton (figure 2.15c). The passive exoskeleton makes use of a passive clutch, that controls the locking and unlocking of the mechanism, and a series spring, that stores energy during stance phase dorsiflexion and releases it at push off. According to their findings, a metabolic cost reduction of $7.2 \pm 2.6\%$ was achieved when compared to walking without the exoskeleton [2]. The active exoskeleton developed by Mooney et al. relies on brushless DC motors connected to winch actuators that act on the struts connecting the shank and the foot. During test trials a metabolic cost reduction of $8 \pm 3\%$ was achieved [4].

The main goal of the passive exoskeleton prototype developed by Collins et al. was to determine if it was possible, and if so, how, to reduce the metabolic rate of walking without providing an additional energy source, that is, by using solely passive components when developing an ankle exoskeleton. The design utilized in their experiments worked with a spring acting in parallel with the calf's muscles which off-loaded the muscle force, leading to a decrease in metabolic energy consumed during walking.

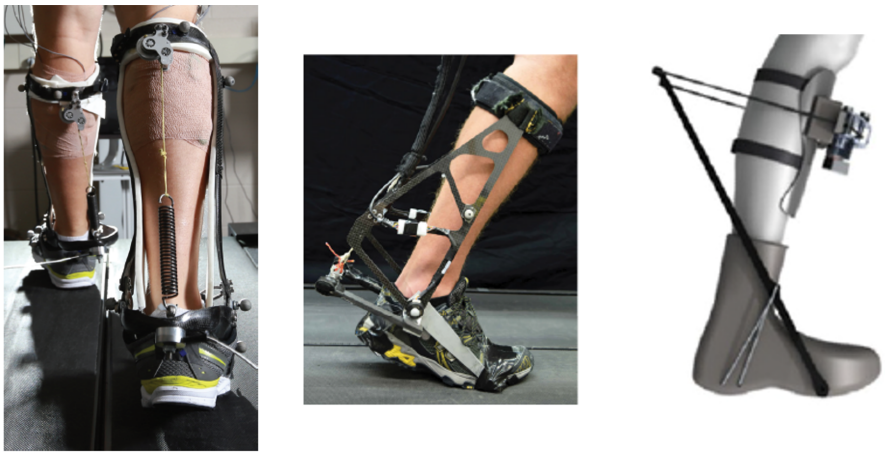

(a) (b) (c)

Figure 2.15: Performance Augmentation Ankle Exoskeletons developed by: (a) Collins et al. [2]; (b) Jackson and Collins [33]; (c) Mooney et al. [4].

The exoskeleton produced a torque pattern similar to that of the ankle, thus reducing the moment produced by the plantarflexors and, consequently, reducing their activation. As expected, this effect was particularly noticeable in the soleus, since this is an uniarticular muscle acting solely on the ankle and so the exoskeleton closely mimics its actuation [34]. Increasing the spring stiffness above a certain threshold (180 Nm/rad) lead to an increase in metabolic cost. It is important to note that, according to the authors, the effective mechanical stiffness of the exoskeleton was about 33% lower than the nominal spring stiffness [2]. This increase in metabolic cost could be due to several factors, such as an increase in dorsiflexor activity, namely of the tibialis anterior, to counteract the added torque [2, 33], or increased knee muscle activity to prevent hyperextension during stance [2].

An increase in plantarflexor activity at the end of stance was also observed, even though the joint moment decreased. This could suggest that the plantarflexors are shortening sub-optimally at the end of stance. Indeed “the plantarflexor muscle–tendon units seem tuned for near-optimal efficiency and power production during unassisted locomotion” [34]. During gait, the muscles produce near isometrical, albeit eccentric force, while the Achilles tendon lengthens, storing mechanical energy. This is an energetically efficient strategy since near isometrical force requires little energy and, at push off, the shortening of the muscles, allied to the tendon’s recoil, generates the required power burst. Moreover, the architecture of the plantarflexor muscle-tendon units allows the “muscle fibers to operate at favorable lengths and velocities during positive work production” [34] at push off. Changes to these fine-tuned muscle-tendon units’ operating ranges can lead to an increase in energy expenditure.

The goal of the active prototype was two-fold: analyse the effect of adding work, and of adding torque, to the biological system. The findings were that “both techniques reduced effort-related measures at the assisted ankle” [33], but while adding work reduced the metabolic cost, adding torque lead to an increase in the energy expended, most likely due to whole body effects [33]. Another possibility for this increase stems from the disturbance of the fine-tuned plantarflexor muscle-tendon units. In order to explore this possibility, the authors conducted further analyses using musculoskeletal models, that is, experimentally

measured EMG and joint kinematics data were used to drive a musculoskeletal model of the soleus muscle [34]. The authors warn that the increase in metabolic rate with added torque would have been hard to predict if models that assumed fixed kinematics or did not include muscles were to have been used.

Chapter 3

Muscle Models

3.1 Hill-type Muscle-Tendon Model

Hill-type muscle models provide a fair description of the dynamic behavior of real muscles and are typically used due to their simplicity and low computational cost [35]. In this section a Hill-type Muscle Tendon Unit (MTU) model, as presented in Geyer and Herr [36], is described.

The MTU model (Figure 3.1) consists of a Contractile Element (CE), representing the muscle fibers, which at rest has zero tension but when activated is able to shorten [37], an elastic series element (SE), representing the stiffness of the tendon, an elastic parallel element (PE), which represents the stiffness of structures parallel to the muscle fibers [38], and a buffer element (BE). The PE is engaged when the CE stretches beyond its optimal length, while the buffer element prevents the collapse of the contractile element if the series element is slack, that is, if $l_{MTU} - l_{CE} < l_{slack}$. l_{MTU} is the length of the Muscle Tendon Unit, l_{CE} is the length of the Contractile Element and l_{slack} is the length of the SE when slack [36].

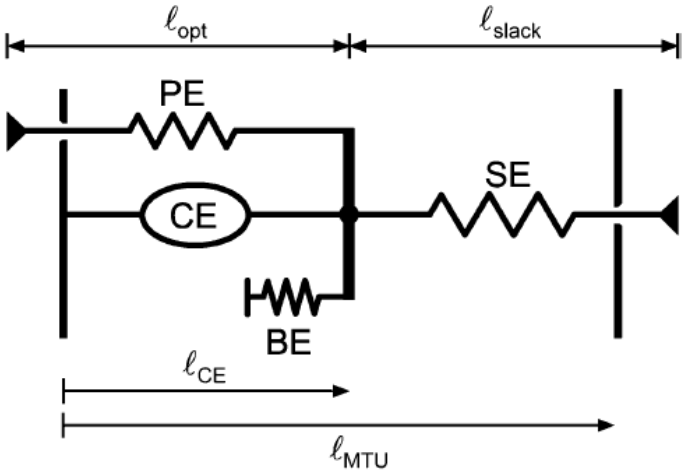

Figure 3.1: Representation of the Muscle Tendon Unit (MTU) [36].

There is a force balance in the MTU, so the force along the series element (F_{SE}), or tendon, is equal to the force along the muscle (F_M), equation 3.1. Since the muscle is composed by the CE, PE and BE,

the muscle force is given by the sum of the force of these elements (equation 3.2). The length of the MTU is given by equation 3.3, where l_{SE} is the length of the tendon.

$$F_{MTU} = F_{SE} = F_M \tag{3.1}$$

$$F_M = F_{CE} + F_{PE} - F_{BE} \tag{3.2}$$

$$l_{MTU} = l_{SE} + l_{CE} \tag{3.3}$$

The force generated by the CE is given by equation 3.4, where f_{max} is the maximal isometric muscle force, $a(t)$ is the muscle's activation and f_l and f_v are the normalized CE intrinsic force-length (*f-l*) and force-velocity (*f-v*) relations [36].

$$F_{CE} = f_{max}\ a(t)\ f_l(l_{CE})\ f_v(v_{CE}) \tag{3.4}$$

The *f-l* curve, defined by equation 3.5 and shown in figure 3.2, peaks at a value of 1 at the optimal fiber length and decreases when the fibers are shorter or longer than that. The width of the curve is defined by w and its amplitude at the extremities is defined by c [35].

$$f_l(l_{CE}) = \exp\left(c\left|\frac{l_{CE} - l_{opt}}{l_{opt}w}\right|^3\right) \tag{3.5}$$

The *f-v* curve, defined by equation 3.6 and shown in figure 3.3, reflects the CE's force production dependence on the fiber's velocity. The force production decreases drastically as shortening velocity increases, until a maximum velocity is reached, at which the CE is no longer able to produce force. During lengthening the fibers resist larger forces, so the curve is scaled by N, which is the dimensionless force reached at maximum velocity. K defines the curvature of the *f-v* curve [39].

$$f_v(v_{CE}) = \begin{cases} \frac{v_{max} - v_{CE}}{v_{max} + K v_{CE}}, & v_{CE} < 0 \\ N + (N-1)\ \frac{v_{max} + v_{CE}}{7.56 K v_{CE} - v_{max}}, & \text{otherwise} \end{cases} \tag{3.6}$$

Here the tendon is considered as a nonlinear elastic element connecting the muscle to the bone. Its force-strain relation is given by equation 3.7, where ϵ_{ref} is the reference strain and ϵ is computed using equation 3.8, in which l_{rest} is the tendon's resting length.

$$F_{SE}(\epsilon) = \begin{cases} \frac{\epsilon}{\epsilon_{ref}^2}, & \epsilon > 0 \\ 0, & \text{otherwise} \end{cases} \tag{3.7}$$

$$\epsilon = \frac{l_{SE} - l_{rest}}{l_{rest}} \tag{3.8}$$

The force of the parallel passive element is given by equation 3.9 and shown in figure 3.2. The force produced by this element is coupled to the *f-l* curve of the CE by parameter w. The force-length relation of the buffer element is given by equation 3.10 and shown in figure 3.2, and is also dependent on w.

$$F_{PE}(l_{CE}) = \begin{cases} f_{max} \left(\frac{l_{CE}-l_{opt}}{l_{opt}w}\right)^2, & l_{CE} > l_{opt} \\ 0, & \text{otherwise} \end{cases} \tag{3.9}$$

$$F_{BE}(l_{CE}) = f_{max} \left(\frac{2(l_{opt} - l_{CE} - w)}{l_{opt}\ w}\right)^2 \tag{3.10}$$

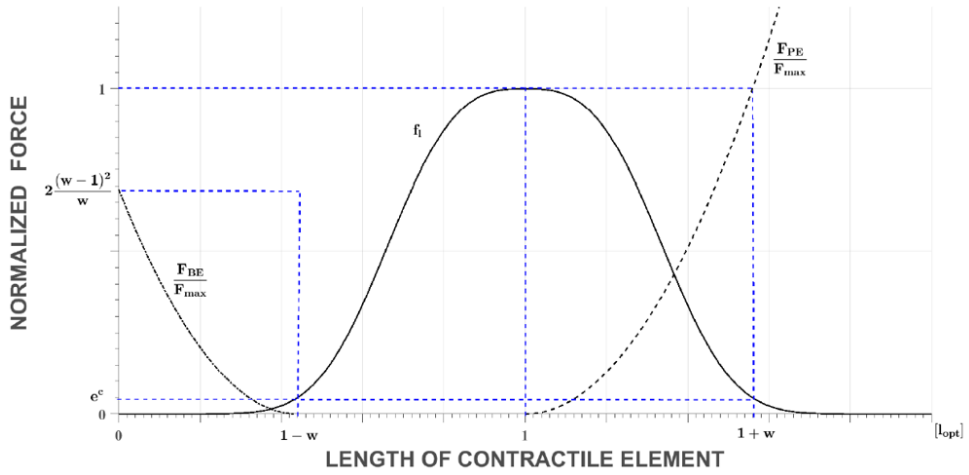

Figure 3.2: *f-l* curve (equation 3.5), normalized force–length relationship of the passive element (equation 3.9), and normalized force-length relationship of the buffer elasticity element (equation 3.10) [35].

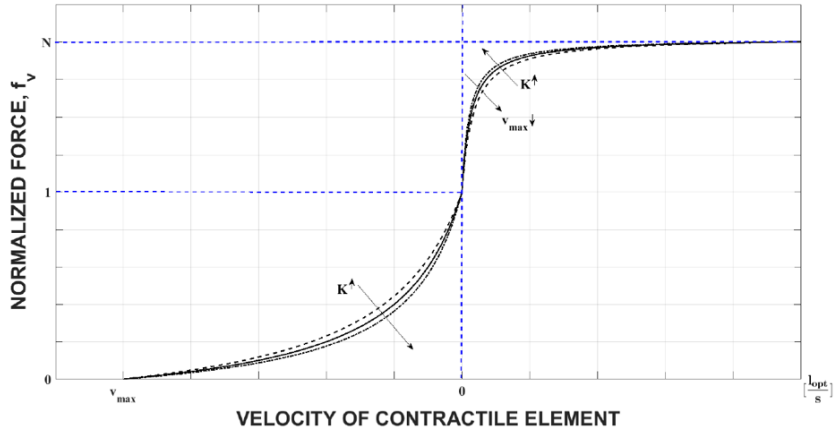

Figure 3.3: *f-v* curve (equation 3.6) [35].

The muscle dynamics are thus described by the equations above and governed by a set of parameters, some muscle specific, which are tabulated values. The values used in this work are presented in table 3.1 [36, 38].

3.2 Muscle Energy Expenditure Model

In this section, a model for muscle energy expenditure, developed by Umberger et al. [17] and used at length by Ackermann [38] in his doctoral thesis, is described. Here, the notation adopted will be

Table 3.1: Muscle specific parameters required by the Hill-type model and by the muscle energy expenditure model. Values for ft obtained from Ackermann [38], all other values obtained from Geyer and Herr [36].

Parameter	l_{slack} [m]	l_{opt} [m]	v_{max} [$l_{opt}s^{-1}$]	f_{max} [N]	ft [%]
Gastrocnemius	0.40	0.05	12	1500	50
Tibialis Anterior	0.24	0.06	12	800	25
Soleus	0.26	0.04	12	4000	20
Parameter	ω	c	N	K	ϵ_{ref}
	0.56	0.05	1.5	5	0.04

that of the doctoral thesis by Ackermann, where the energy expenditure model was used in order to develop a cost function for static optimization which takes into account the metabolic cost. In this work, the metabolic cost of walking with different foot prosthesis was also estimated based on computational simulations. In a recent study by Gonabadi et al. [18], this same model was coupled to a Hill-type muscle model in order to study the energy expended by eight muscles of the lower limb for walking under different conditions. In their research, Jackson et al. [34] applied Umberger's model to previously acquired data of subjects walking with an ankle exoskeleton, in order to estimate its effect on individual muscle's metabolic rates.

This model was chosen since it is founded on mammalian and human muscle experimental data and it accurately "accounts for muscle heat production during submaximal and eccentric muscle activities [38]". This model later suffered revisions [40], and negative work was excluded from the summation and the lengthening heat rate coefficient (α_L) was redefined. However, according to Uchida et al. [41] negative mechanical work should be included and thus the original definition of α_L kept. Indeed, most research developed using this model follows the formulation of Uchida et al. [18, 34].

The total rate of muscle energy expenditure ($\dot{E}$) can be expressed as a sum of four terms, as seen in Equation 3.11. These terms are: the activation heat rate ($\dot{h}_a$), the maintenance heat rate ($\dot{h}_m$), the shortening/lengthening heat rate ($\dot{h}_{sl}$) and the mechanical work rate of the contractile element ($\dot{w}_{ce}$).

$$\dot{E} = m_{musc} \times (\dot{h}_a + \dot{h}_m + \dot{h}_{sl}) + \dot{w}_{ce} \tag{3.11}$$

The mechanical work rate of the Contractile Element (CE) is given by equation 3.12, where f_{ce} and v_{ce} are the force and velocity of the CE, respectively. Positive mechanical work corresponds to concentric contraction (negative v_{ce}), while negative mechanical work corresponds to eccentric contraction [9].

$$\dot{w}_{ce} = -f^{ce} v^{ce} \tag{3.12}$$

For computational purposes Ackermann [38] sums all muscle heat rates into the specific muscle heat rate ($\dot{h}$):

$$\dot{h} = \dot{h}_a + \dot{h}_m + \dot{h}_{sl} \tag{3.13}$$

It is important to note that the total heat rate ($\dot{h}$) cannot fall below $1\ Wkg^{-1}$, since this is the resting energy rate for human skeletal muscle *in vivo*. With the expressions obtained for $\dot{w}_{ce}$ (equation 3.12) and for $\dot{h}$ (equation 3.13), the expression for the total rate of muscle energy expenditure ($\dot{E}$), given in Watt (W), can be rewritten as:

$$\dot{E} = -f^{ce}v^{ce} + m_{musc}\dot{h} \tag{3.14}$$

The muscle's mass (m_{musc}) is related to the Physiological Cross-Sectional Area (PCSA) of the muscle and the optimal CE length (l^{ce}_{opt}) by equation 3.15 [38], where ρ^m is the muscle density, which is $1059.7\ kg\ m^{-3}$ for mammalian muscle. Since the PCSA is related to the maximal isometric muscle force (f_{max}) by equation 3.16, where $\bar{\sigma}$ is the specific tension of the muscle, with a value of $0.25\ MPa$ in this model, it is possible to obtain the muscle mass as a function of the optimal CE length and the maximal isometric muscle force (equation 3.17), which are tabulated muscle parameters (table 3.1).

$$m_{musc} = \rho^m l^{ce}_{opt} PCSA \tag{3.15}$$

$$f_{max} = \bar{\sigma} PCSA \tag{3.16}$$

$$m_{musc} = \frac{\rho^m l^{ce}_{opt}}{\bar{\sigma}} f_{max} \tag{3.17}$$

In order to compute the specific muscle heat rate ($\dot{h}$) it is necessary to compute all its parts. The activation ($\dot{h}_a$) and maintenance ($\dot{h}_m$) heat rates can be lumped together ($\dot{h}_{am}$). The activation heat rate is associated with the sarcoplasmic reticular ion transport, a process which is triggered by activation, while the maintenance heat rate is related to actomyosin interactions [17]. $\dot{h}_{am}$ is linearly related to the percentage of Fast Twitch (FT) muscle fibers (ft) by equation 3.18. Theoretically, a human muscle composed solely of fast twitch fibers would have a $\dot{h}_{am}$ of $153\ Wkg^{-1}$, while for a muscle with only Slow Twitch (ST) fibers this value would be $25\ Wkg^{-1}$.

$$\dot{h}_{am} = 1.28 \times ft + 25 \tag{3.18}$$

The shortening and lengthening heat rates, both related to actomyosin interactions, can be lumped together into $\dot{h}_{sl}$ by considering two cases [17]. One for shortening, that is, when the velocity of the contractile element ($\tilde{v}^{ce}$) is negative, and one for lengthening, when $\tilde{v}^{ce}$ is positive. Note that $\tilde{v}^{ce} = v^{ce}/l^{ce}_{opt}$ and is expressed in $l^{ce}_{opt}s^{-1}$.

The shortening heat rate production is classically modeled as the product of a coefficient (α_s) and $\tilde{v}^{ce}$. In this model a distinction is made between shortening heat rate ($\dot{h}_s$) for slow twitch and fast twitch fibers by taking into account that the total heat rate for ST fibers shortening at their maximal velocity ($\tilde{v}^{ce}_{max,st}$) is approximately 5 times greater than their $\dot{h}_{am}$, while it is only 1.5 - 3 times greater in the case of FT fibers. Considering this, the shortening heat coefficients for slow twitch and fast twitch fibers are computed using equations 3.19 and 3.20, respectively.

$$\alpha_{s,st} = \frac{4 \times 25 \times 2.5}{\tilde{v}^{ce}_{max,ft}} = \frac{250}{\tilde{v}^{ce}_{max,ft}} \tag{3.19}$$

$$\alpha_{s,ft} = \frac{153}{\tilde{v}^{ce}_{max,ft}} \tag{3.20}$$

$$\tilde{v}^{ce}_{max,ft} = 12\ l^{ce}_{opt}\ s^{-1} \tag{3.21}$$

The denominator for both these equations is the maximal velocity of fast twitch fibers (equation 3.21). Since $\tilde{v}^{ce}_{max,st} = 2.5 \times \tilde{v}^{ce}_{max,ft}$ the numerator of equation 3.19 reflects this substitution and takes into account the relation between $\dot{h}_s$ and $\dot{h}_{am}$ by multiplying its value for slow twitch fibers ($25\ Wkg^{-1}$) by a proportion of 4. The numerator for equation 3.20 takes into account this relationship by multiplying $\dot{h}_{am}$ for slow twitch fibers ($153\ Wkg^{-1}$) by a proportion of 1. The rate of heat production during lengthening can also be modeled as a product between a coefficient (α_l) and $\tilde{v}^{ce}$. This coefficient is given by equation 3.22.

$$\alpha_l = 4\ \alpha_{s,st} \tag{3.22}$$

The final expression for the shortening and lengthening heat rate ($\dot{h}_{sl}$) is given by equation 3.23.

$$\dot{h}_{sl} = \begin{cases} -\alpha_{s,st}\ \tilde{v}^{ce}\ (1 - ft/100) - \alpha_{s,ft}\ \tilde{v}^{ce}(ft/100), & \text{if } \tilde{v}^{ce} \leq 0 \\ \alpha_l\ \tilde{v}^{ce}, & \text{if } \tilde{v}^{ce} > 0 \end{cases} \tag{3.23}$$

In this model, it is assumed that the first term of the right hand side of the shortening heat rate does not exceed $100\ Wkg^{-1}$ (equation 3.24). This is the same as assuming that the slow twitch fibers continue to release energy at the maximal rate if the muscle is shortening faster than the maximal velocity for ST fibers. In reality this is unlikely to occur [17].

$$-\alpha_{s,st}\ \tilde{v}^{ce}(1 - ft/100) \leq 100\ Wkg^{-1} \tag{3.24}$$

In order to achieve appropriate activation dependence, the following scaling factors dependent on the activation (a_m) are used: $a_{am} = a_m^{0.6}$ scales the activation and maintenance heat rate and $a_s = a_m^2$ scales the shortening and lengthening heat rates when $\tilde{v}^{ce} \leq 0$, while $a_s = a_m$ scales it when $\tilde{v}^{ce} > 0$. Another scaling factor that must be taken into account has to do with aerobic versus anaerobic metabolism. The molar enthalpy change is greater by a factor of two for aerobic conditions, however no submaximal activity is strictly aerobic. Therefore, a scaling factor $S = 1.5$ is used for primarily aerobic conditions while $S = 1$ is used for anaerobic conditions. Since gait is primarily aerobic $S = 1.5$ was adopted in this work.

In addition to these scaling factors, another is needed to account for the length dependence of $\dot{h}_m$ (which is 60% of $\dot{h}_{am}$) and $\dot{h}_{sl}$. Both these quantities are near maximal at l^{ce}_{opt} and decrease with the *f-l* curve for lengths beyond l^{ce}_{opt}, but for shorter lengths there is little change in these heat rates. Thus, for

$l^{ce} > l^{ce}_{opt}$ both quantities are scaled by the isometric force-length relation, that is the *f-l* curve (f_l).

Once all the parameters, scaling factors and equations are defined the specific muscle heat rate is given by equation 3.25.

$$\dot{h} = \begin{cases} \dot{h}_{am}\, a_m^{0.6}\, S + \begin{cases} [-\alpha_{s,st}\, \tilde{v}^{ce}\, (1 - ft/100) - \alpha_{s,ft}\, \tilde{v}^{ce}\, (ft/100)]\, a_m^2\, S, & \text{if } \tilde{v}^{ce} \leq 0 \\ \alpha_l\, \tilde{v}^{ce}\, a_m\, S, & \text{if } \tilde{v}^{ce} > 0 \end{cases}, & \text{if } l^{ce} \leq l^{ce}_{opt} \\ (0.4 + 0.6\, f_l)\, \dot{h}_{am}\, a_m^{0.6}\, S + \begin{cases} [-\alpha_{s,st}\, \tilde{v}^{ce}\, (1 - ft/100) - \alpha_{s,ft}\, \tilde{v}^{ce}\, (ft/100)]\, f_l\, a_m^2\, S, & \text{if } \tilde{v}^{ce} \leq 0 \\ \alpha_l\, \tilde{v}^{ce}\, f_l\, a_m\, S, & \text{if } \tilde{v}^{ce} > 0 \end{cases}, & \text{if } l^{ce} > l^{ce}_{opt} \end{cases} \tag{3.25}$$

The value of the specific muscle heat rate, along with the muscle mass and the CE velocity and force, are then input in equation 3.14 to obtain the total energy rate of the muscle for each time instant. While "eccentric muscle work can be performed more efficiently than an equivalent amount of concentric work and can perhaps even cause a net absorption of heat, studies have shown that active lengthening cannot result in a net synthesis of ATP" [16]. Thus, the total instantaneous power ($\dot{E}$) is prevented from becoming negative, that is, $\dot{E} \geq 0$ for every instant [41]. Finally, integrating this quantity over time, for each muscle, yields the total energy expenditure required to produce the movement. The total metabolic cost (J/kg) is given by equation 3.26, while per meter walked ($J/kg/m$) it is given by equation 3.27. T is the motion duration, m the subject's mass, and v the walking speed [15]. The average metabolic power consumption, in W/kg, is given by equation 3.28 [42].

$$E_{tot} = \frac{1}{m} \int_{t=0}^{T} \sum_{i=1}^{N_{musc}} \dot{E}_i\, dt \tag{3.26}$$

$$E_{tot} = \frac{1}{Tmv} \int_{t=0}^{T} \sum_{i=1}^{N_{musc}} \dot{E}_i\, dt \tag{3.27}$$

$$\bar{P}_{avg} = \frac{1}{Tm} \int_{t=0}^{T} \sum_{i=1}^{N_{musc}} \dot{E}_i\, dt \tag{3.28}$$

Chapter 4

Dynamics of the Ankle Joint

4.1 Problem Formulation

This dissertation aims to analyse the effect of an ankle exoskeleton on the energetics of the ankle joint. For that, a computational model of the ankle musculoskeletal complex is developed, where a linear stiffness spring is added to the joint. The computational model is implemented in Matlab and has two different versions. The first considers the two main plantar flexor muscles, soleus and gastrocnemius, and the main dorsiflexor, the tibialis anterior. And the second one considers solely the soleus and the tibialis anterior.

4.2 Methodology

4.2.1 Reference Gait Model and Data

Data for the ankle joint kinematics was obtained from the Neuromuscular Locomotion Model developed by Geyer [36, 39]. This model, implemented in Simulink, has seven segments driven by 14 muscles, which are modeled as Hill-type muscles (figure 4.1) [43]. The model simulates walking at a speed of 1.3 m/s, and the soleus, gastrocnemius and tibialis anterior were considered for energy cost.

The data retrieved from the simulation were the ankle joint angle, the total moment produced at the joint (figure 4.2), as well as the activation, length of the muscle tendon unit (l_{mtu}) and velocity of the contractile element (v_{ce}) of each muscle considered (figure 4.3).

4.2.2 Energetic Ankle Model

The muscles are modeled using the Hill-type muscle model described in detail in chapter 3.1, coupled to the energetic model described in chapter 3.2. This approach allows for the estimation of the energy expenditure of each individual muscle considered in the analysis.

The Hill-type muscle model describes the muscle's mechanics, that is, from the length of the MTU and the activation, it estimates the force of the contractile element (f_{ce}), its velocity (v_{ce}) and length (l_{ce})

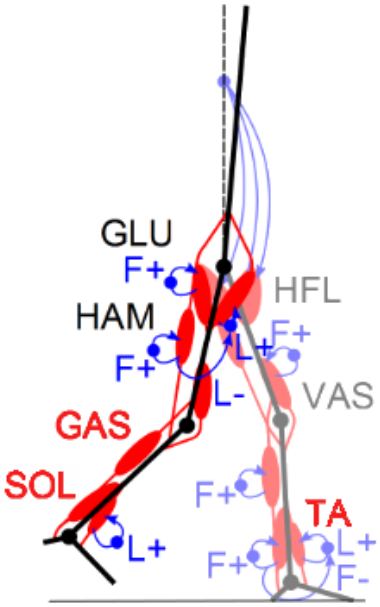

Figure 4.1: Neuromuscular Locomotion Model developed by Geyer et al. Labeled in red are the muscles relevant for this work: soleus, gastrocnemius and tibialis anterior. Adapted from Song and Geyer [43].

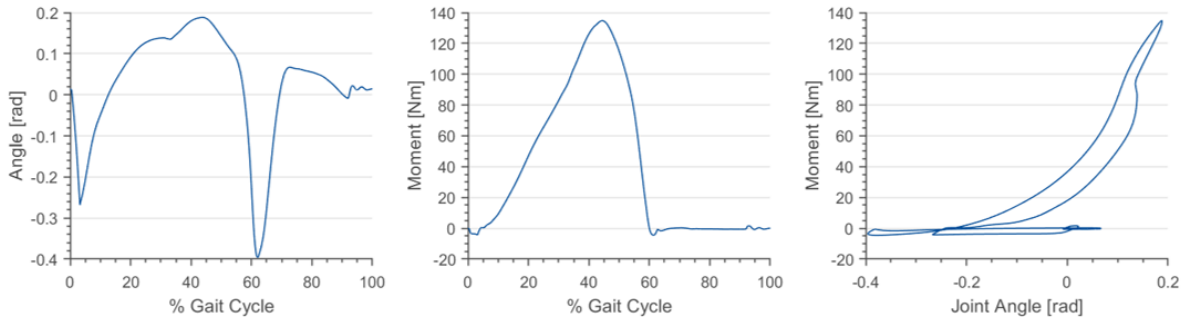

Figure 4.2: Data retrieved from the Neuromuscular Locomotion Model. From left to right: ankle joint angle along the gait cycle; total moment produced at the joint along the gait cycle; total moment vs joint angle curve.

at every instant of the movement. As seen in section 3.1, the model requires certain input parameters, some muscle specific: l_{slack}, l_{opt}, v_{max} and f_{max}, and others that define the *f-l*, *f-v* and tendon curves (table 3.1). Since the considered model only accounts for the soleus, gastrocnemius and tibialis anterior, the muscle specific parameters were retrieved solely for these muscles. The muscle-tendon model was implemented in Simulink. The implementation was adapted from the Neuromuscular Locomotion Model, described above [36, 39]. Only the Simulink blocks corresponding to the Hill-Type muscle-tendon units of the muscles of interest were kept for this work. Each block receives as input the activation and MTU length of its corresponding muscle and outputs the velocity, length and force of the Contractile Element, as well as the length of the tendon.

The muscle energy expenditure model computes the average power (equation 3.28) and total energy expenditure (equations 3.26 and 3.27) of the muscle given the force, velocity and length of the contractile

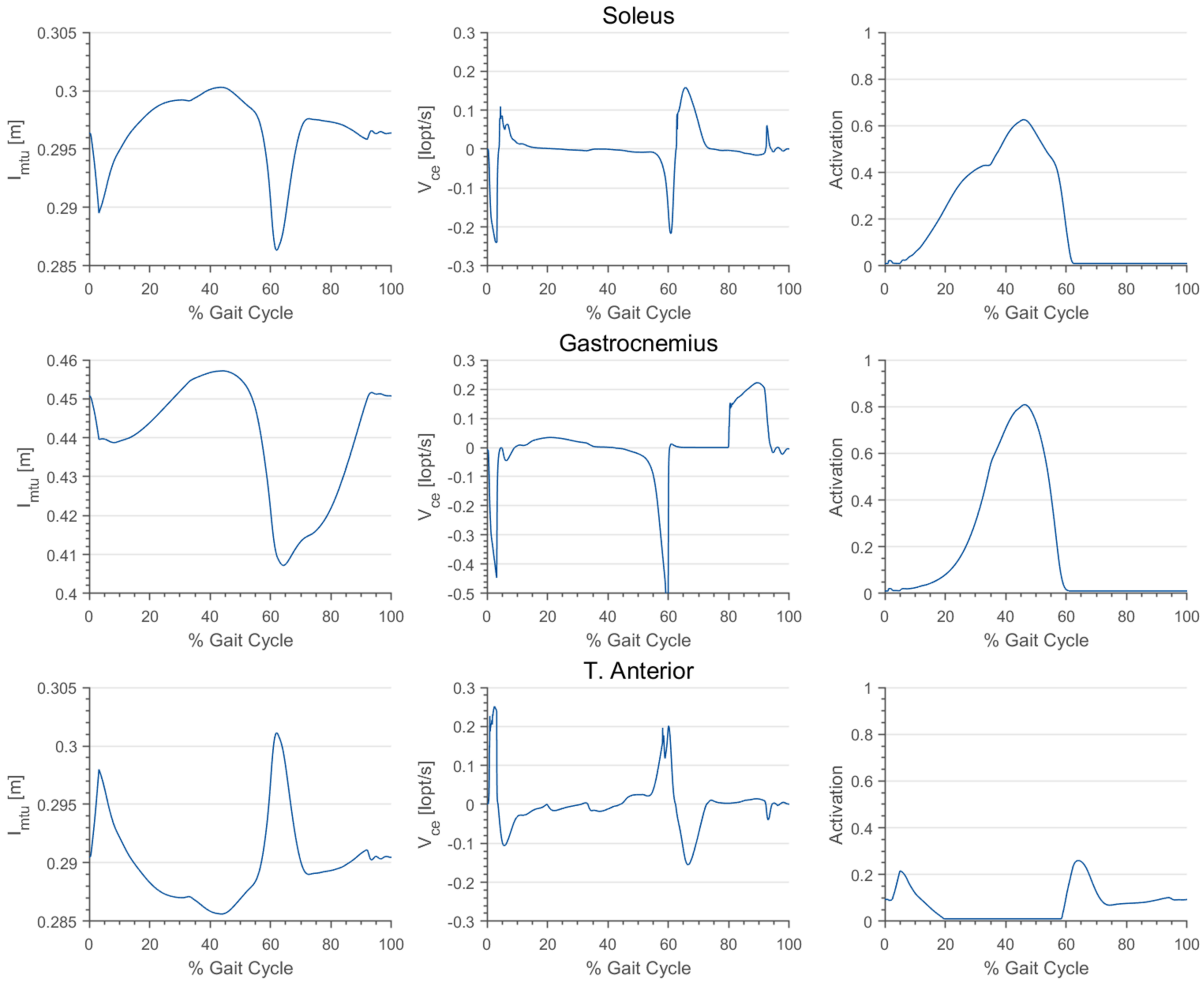

Figure 4.3: Data retrieved from the Neuromuscular Locomotion Model for each muscle considered. From left to right: l_{mtu} along the gait cycle; v_{ce} along the gait cycle; muscle activation along the gait cycle.

element and the activation. In addition to these, the model also provides the time profile of: the mechanical work rate ($\dot{w}_{ce}$), the shortening-lengthening heat rate ($\dot{h}_{sl}$), the activation and maintenance heat rate ($\dot{h}_{am}$) and of the metabolic power ($\dot{E}$). All required variables, except for the activation, are obtained for each instant from the MTU model. This model also requires several muscle specific parameters: l_{opt}, v_{max}, f_{max} and ft (table 3.1). The energy expenditure model was implemented in Matlab, as a function. Which receives as input the parameters and variables required and outputs the aforementioned values, computed resorting to the equations described in chapter 3.2. The workflow of this process is illustrated in figure 4.4.

In the considered exoskeleton approach, the spring stores energy during the stance phase dorsiflexion and releases it at push off [5]. When it is active, a reduction in the energy expended by the ankle's muscles is expected, owing to a reduction in torque. In order to emulate this behavior, the spring added to the model is activated in the instant controlled dorsiflexion begins and deactivated once the ankle joint angle reaches the same angle as when it was activated, figure 4.5 illustrates this behavior. As previously stated, the spring added to the model has linear stiffness. Thus, the moment produced by the spring is given by equation 4.1, where K_s is the spring's stiffness, θ_0 is the joint angle at spring activation and θ

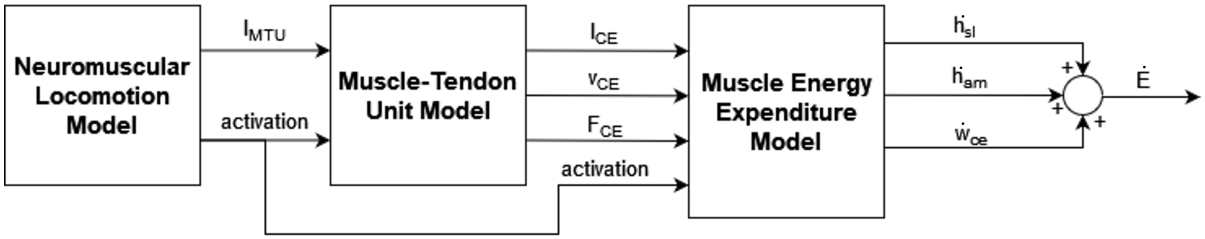

Figure 4.4: Workflow of the musculoskeletal and energetic model implemented. The activation and l_{mtu} are obtained from the Neuromuscular Locomotion Model and input in the MTU model. This in turn computes the l_{ce}, v_{ce} and F_{ce}, which are used by the muscle energy expenditure model do compute the total energetic cost.

is the instantaneous joint angle.

$$M_{spring} = K_s(\theta - \theta_0) \tag{4.1}$$

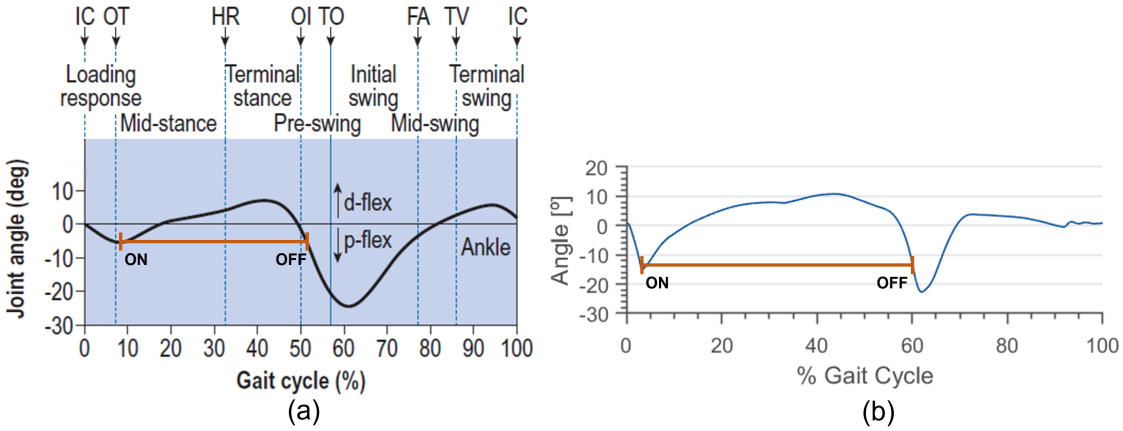

Figure 4.5: Ankle Joint ankle and instants at which the spring is activated and deactivated. (a) Reference curves for the ankle joint angle, adapted from Whittle [7]; (b) joint angle retrieved from the Neuromuscular Locomotion Model.

4.2.3 Optimization

As previously mentioned, when active, the spring added to the ankle model produces a moment. Admitting that the movement of the ankle joint is not altered by the effect of the spring, that is, that the kinematics remain the same, the total moment of the ankle complex will remain the same. Thus, the moment generated by the muscles active during this period, the triceps surae, which are contracting eccentrically during controlled dorsiflexion and concentrically during PO, will be reduced compared to when the spring is not active. A reduction of the energy expended by the triceps surae is expected to be associated with this decrease in moment produced.

The total reduction in moment produced by the muscles is trivial to obtain, as the sum of the moment produced by the muscles must be equal to that produced before the spring was introduced, minus the moment produced by the spring. This is expressed mathematically by equation 4.2, where M_m is the moment produced by the given muscle, M_D is the moment obtained from the muscle dynamics without the spring and M_{spring} is the spring's moment.

$$\sum_{m=1}^{2}(M_m) = M_D - M_{spring} \tag{4.2}$$

The same is not true for computing the expended energy, which depends on a multitude of factors and will be influenced by the reduction in muscle moment production. Most importantly, since the muscles are producing less moment, and hence less force, the activation will be reduced. Once the reduced activation is obtained it can be input, along with the MTU length, in the ankle complex model in order to ascertain if there is a reduction in muscle energy expenditure due to the presence of the spring. In order to compute the reduction in muscle activation, optimization strategies must be employed.

Multiobjective Dynamic Optimization

Dynamic optimization allows the dynamic behavior of the Muscle Tendon Unit as a whole to be considered, whereas static optimization suffices when the tendon is neglected. Routines for multiobjective optimization implemented in Matlab's Optimization Toolbox allow for the optimization of parameters in Simulink models [44]. While taking into account the tendon's behavior and the dynamic aspects of the MTU, this optimization strategy fails in an important aspect. Since it is unable to make use of a biologically relevant objective function, it does not allow for the solution of the redundancy problem. Therefore, the devised multiobjective optimization was used to provide an analysis of a single agonistic muscle and not of the triceps surae as a whole. The muscle where the impact of the exoskeleton is more relevant is the soleus, as it is the uniarticular muscle acting at the ankle joint during stance phase dorsiflexion [34]. Indeed, as illustrated in figure 4.6, the soleus produces most of the moment generated at the joint during stance phase. Thus, restricting the energetic analysis to this muscle is a valid approximation of the physiological phenomenon.

Figure 4.6: Moment generated at the ankle joint during the gait cycle. From left to right: total moment; moment produced by the soleus; moment produced by the gastrocnemius. Dark blue represents the stance phase and light blue the swing phase.

As stated before, the Hill-Type Muscle Tendon Unit model used in this work was implemented in Simulink, and has the activation of the muscle as one of its inputs. Therefore, a multiobjective optimization routine allows for the optimization of the activation based on a certain objective function. In the case of a non-linear least-squares problem, which was the formulation selected for this optimization routine, the objective function comes in the form of a difference between two values that should be minimized. In this case, the difference to minimize is that between the moment produced by the muscle and the moment obtained from the muscle dynamics without the spring, minus the spring's moment. This is translated by equation 4.3, where M_{soleus} is computed as in equation 4.4, where F^m is computed by the MTU model and b^m is the arm of the force, obtained from the Neuromuscular Locomotion Model [36, 39]. M^I_{soleus} is the moment initially generated by the soleus and M_{spring} is computed as in equation 4.1.

$$M_{soleus} - (M^I_{soleus} - M_{spring}) \tag{4.3}$$

$$M_{muscle} = F^m \times b^m \tag{4.4}$$

To make this procedure more time efficient, the state variables of the optimization problem are the activations at twenty, equally spaced points in time, instead of the activations at every time step of the simulation. For numerically stability, the activations are bounded in the interval [0.01; 0.99] as opposed to [0; 1]. For more accurate results, the objective function is computed at all time steps, by inputing the force, computed by the muscle-tendon model, in equation 4.4. The multiobjectives are the values of the objective function at each time step, which are to be minimized.

With the increase in spring stiffness there will be periods in which the moment generated by the spring is higher than that initially generated by the soleus. Therefore, in order for the kinematics to remain unchanged, the stance phase antagonists, particularly the Tibialis Anterior (TA), will have to compensate for this moment which is being added to the joint. In order to emulate this behavior, the same multiobjective optimization approach used for computing the activation of the soleus was used, with some changes to account for the different behavior of the antagonist, to compute the activation of the TA. The objective function is now given by equation 4.5, where M_{TA} is computed as in equation 4.4, M^I_{TA} is the moment initially generated by the Tibialis Anterior, that is, before the spring is introduced and M_{Excess} is the moment the spring produces that exceeds the initial moment generated by the soleus, and is computed according to equation 4.6.

$$M_{TA} - (M^I_{TA} + M_{Excess}) \tag{4.5}$$

$$M_{Excess} = M_{spring} - M^I_{soleus} \tag{4.6}$$

Once the activations of the muscles are obtained they can be input in the ankle complex model, along with the MTU lengths, in order to obtain the energetic cost associated with the motion when the spring is present.

Chapter 5

Results

The developed ankle complex model, comprised of the soleus and tibialis anterior, was applied, together with the multiobjective optimization approach, to the data generated by the Neuromuscular Locomotion Model [36, 39] for the ankle joint. The workflow, represented in figure 5.1, was the following:

- the ankle complex model was run without any stiffness added to the joint, so that the moment generated by each muscle could be saved as the initial muscle moment, M^I_{muscle};
- a given stiffness was added to the model and the multiobjective dynamic optimization routine was used to obtain the muscles' activations;
- the obtained activations and Muscle Tendon Unit lengths are input in the ankle complex model to compute the changes in the muscles' mechanics and energetics.

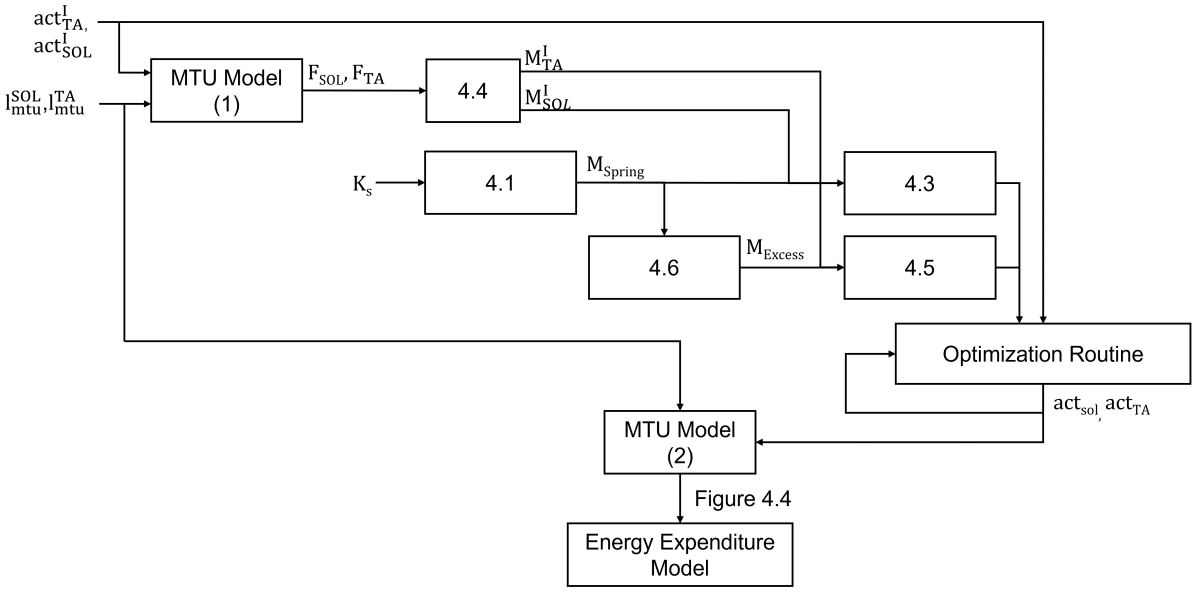

Figure 5.1: Block diagram representation of the dynamic optimization procedure. The numbering represents the equations presented in section 4.2.3.

Seven different values of spring stiffness (K_s) were tested: 50 Nm/rad, 75 Nm/rad, 100 Nm/rad, 125 Nm/rad, 150 Nm/rad, 175 Nm/rad, 200 Nm/rad; and compared to the instance where no stiffness was added to the joint. Results were only analysed for the stance phase, since the spring is only active during this phase and thus, any changes to the muscles' mechanics and energetics occurring during swing are due to numerical instabilities and should not be considered in the analysis.

5.1 Optimization

The activation is the only parameter of the muscle-tendon model which is manipulated in this analysis, as the MTU length is equal for all K_s values, since kinematics are fixed. Therefore, the proper estimation of the activation is crucial to the validity of the results obtained. As previously mentioned, multiobjective optimization is used to compute the activation, required by each muscle, to produce the moment which offsets the one produced by the spring.

In figure 5.2 the moments required from each muscle, for each value of K_s tested, are presented on the left. These moments are computed according to the equations presented in section 4.2.3. The optimal solutions for the moments generated by each muscle are presented next and on the right the activations that lead to the required moments are shown.

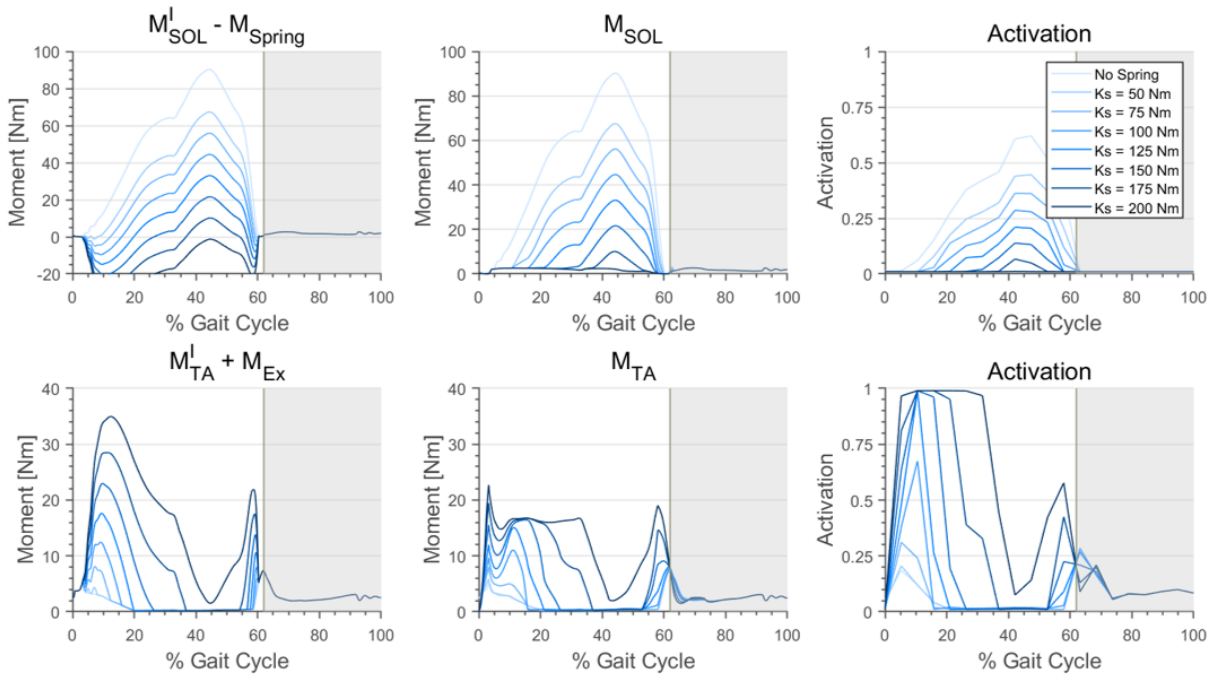

Figure 5.2: Optimization routine, from left to right: moment required from each muscle; optimal solution reached, activations required to produce said moments. On top results for the soleus and below for the tibialis anterior, darker blue indicates higher spring stiffness.

As spring stiffness increases, less moment is required from the plantarflexor and more moment is required from the dorsiflexor. Analysing the curves for $M^I_{SOL} - M_{Spring}$, it is possible to see that the moment required from the soleus for certain periods of stance is negative. Particularly, for K_s = 200 Nm/rad,

no positive moment is required from this muscle. Since muscles cannot produce negative moment, this moment must be provided by its antagonist, the tibialis anterior. This is, indeed, what is shown for the $M_{TA}^{I} + M_{Ex}$ curves. As spring stiffness increases, the moment required from the tibialis anterior is greater. It is also noticeable that, for $K_s > 125$ Nm/rad, during early and mid-stance the moment generated by the TA is not enough to offset the extra moment produced by the spring, even though its activation is maximal.

In figure 5.3 the moment produced by the spring, by the two muscles and the total moment at the joint are presented. Total muscle moment at the joint is computed according to equation 5.1, the TA's moment is subtracted since it is antagonistic to the movement. As spring stiffness increases the moment required from the muscles spanning the joint decreases. The total moment at the joint is the sum of the total muscle moment and the moment produced by the spring (equation 5.2). As expected, given that the kinematics are fixed, the variation in total joint moment across stiffness conditions is negligible, and likely due to numerical instabilities in the optimization procedure.

$$M_{muscles}^{T} = M_{soleus} - M_{TA} \tag{5.1}$$

$$M^{T} = M_{muscles}^{T} + M_{Spring} \tag{5.2}$$

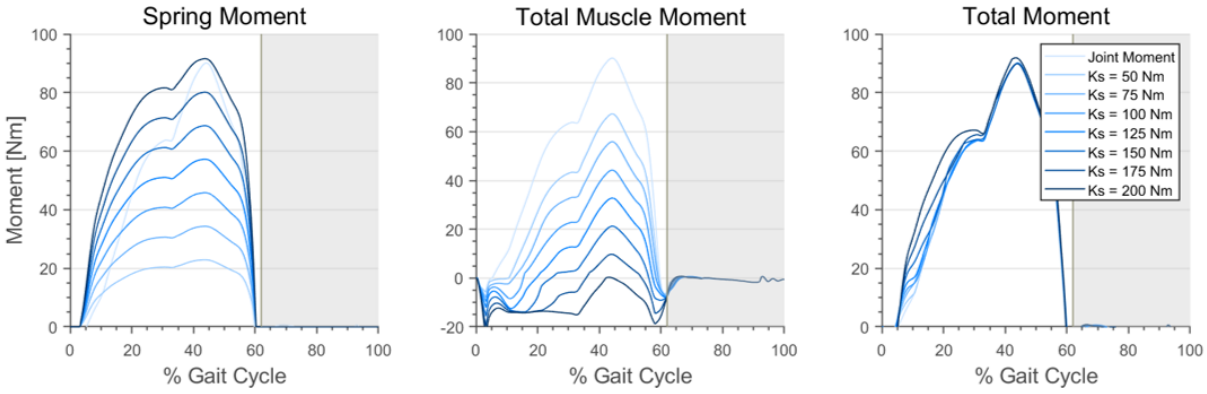

Figure 5.3: Moments, from left to right: produced by the spring; produced by the two muscles; produced at the joint. Darker blue indicates higher spring stiffness.

5.2 Ankle Complex Model

Once the activation values obtained through the optimization routine are validated, they can be input in the developed ankle complex model, in order to analyse the resulting changes in mechanics and energetics of the muscles considered in the model.

As mentioned in section 4.2.2, the Hill-type muscle model computes the mechanics of the MTU, which are then used, along with the activation, by the muscle energy expenditure model to compute the metabolic cost of the movement. The muscle energy expenditure model provides the average value of

each of its portions, as well as the metabolic cost, while the Hill-type muscle model provides the time profiles of the variables it computes. Through the analysis and comparison of these results, the influence of the spring on the ankle complex muscles can be described.

5.2.1 Soleus

As previously stated, the soleus is the muscle which the exoskeleton most closely resembles. It is, therefore, the muscle which should benefit the most from the moment being added to the joint. Indeed, the force required of the plantarflexor, and thus its activation, decrease steadily with the increase in spring stiffness (figure 5.4ab). Another change brought on by the exoskeleton is the increase in Contractile Element (CE) length (l_{ce}) during controlled dorsiflexion (figure 5.4c), which naturally leads to a decrease in tendon length (l_{se}) during the same period (figure 5.4d), since the length of the MTU remains unchanged. This increase in length causes the lengthening velocity of the CE (v_l^{ce}) to increase, since it has to lengthen more in the same time period. But it also leads to an increase in shortening velocity (v_s^{ce}), because at push off the CE is more distended, so it has to contract faster (figure 5.4e).

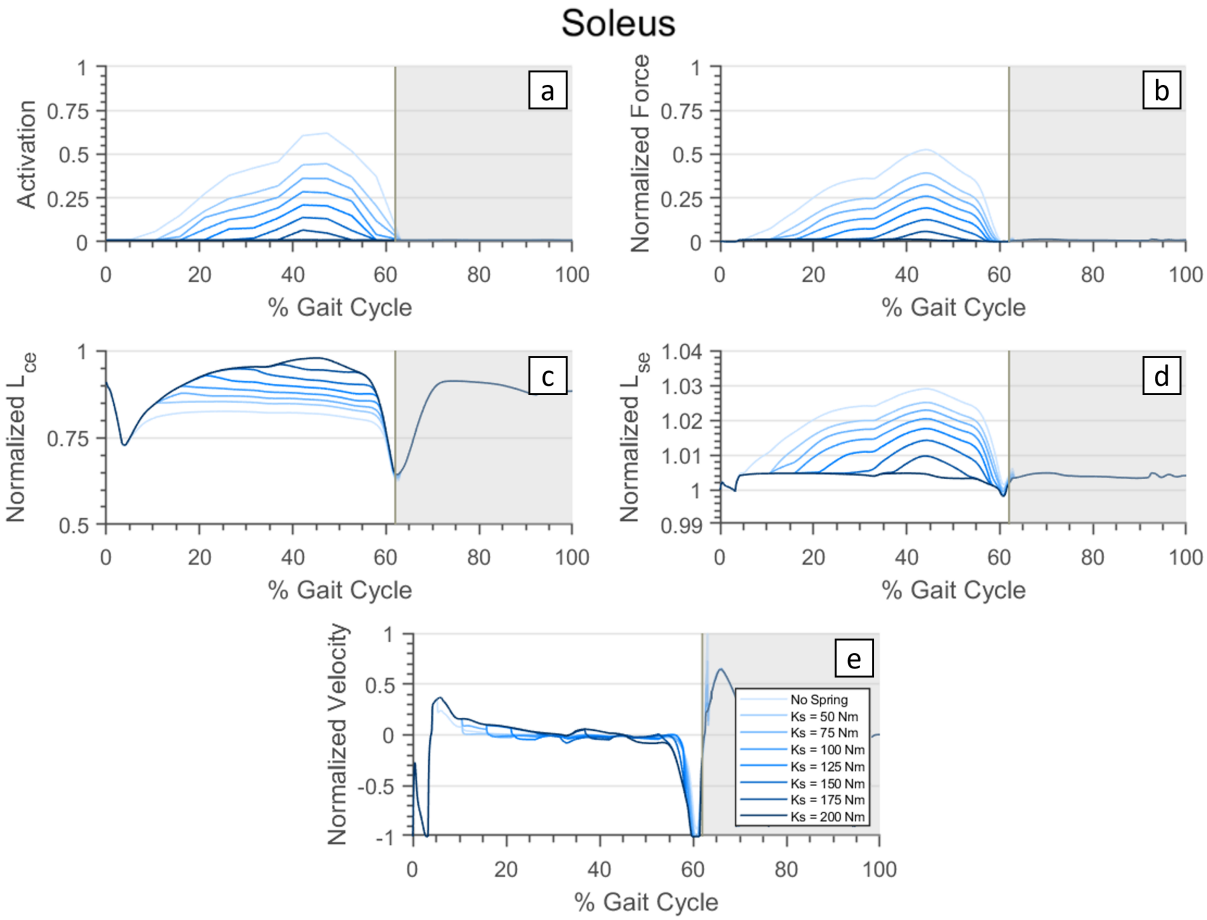

Figure 5.4: Time profiles for the mechanics of the soleus. Darker blue indicates higher spring stiffness.

Initially, the averages of all portions of the muscle energy expenditure rate ($\dot{E}$) decrease with increasing spring stiffness (figure 5.5). But, while the activation and maintenance heat rate ($\dot{h}_{am}$) and the

positive work rate ($\dot{w}_{pos}$) averages always decrease, the shortening and lengthening heat rate ($\dot{h}_{sl}$) and the negative work rate ($\dot{w}_{neg}$) averages start to increase after a certain threshold of K_s is reached. For $\dot{h}_{sl}$ this threshold is $K_s > 100$ Nm/rad, while for $\dot{w}_{neg}$ it is $K_s > 50$ Nm/rad.

The analysis of the equations that rule the energy expenditure model, explains the behavior observed. $\dot{h}_{am}$, computed through equation 3.18, depends only on ft and is scaled by the activation (equation 3.25). Since ft is a fixed value for the given muscle, the value of $\dot{h}_{am}$ depends only on the activation, which decreases with the increase in stiffness (figure 5.4a). On the other hand, $\dot{h}_{sl}$, which is computed through equation 3.23, depends on both ft and the velocity of the contractile element (v^{ce}), and is, once again, scaled by the activation. Both v_l^{ce} and v_s^{ce} increase, on average, with K_s (figure 5.6). So, after the threshold is reached, the decrease in activation does not compensate for the increase in Contractile Element velocity imposed by the added stiffness.

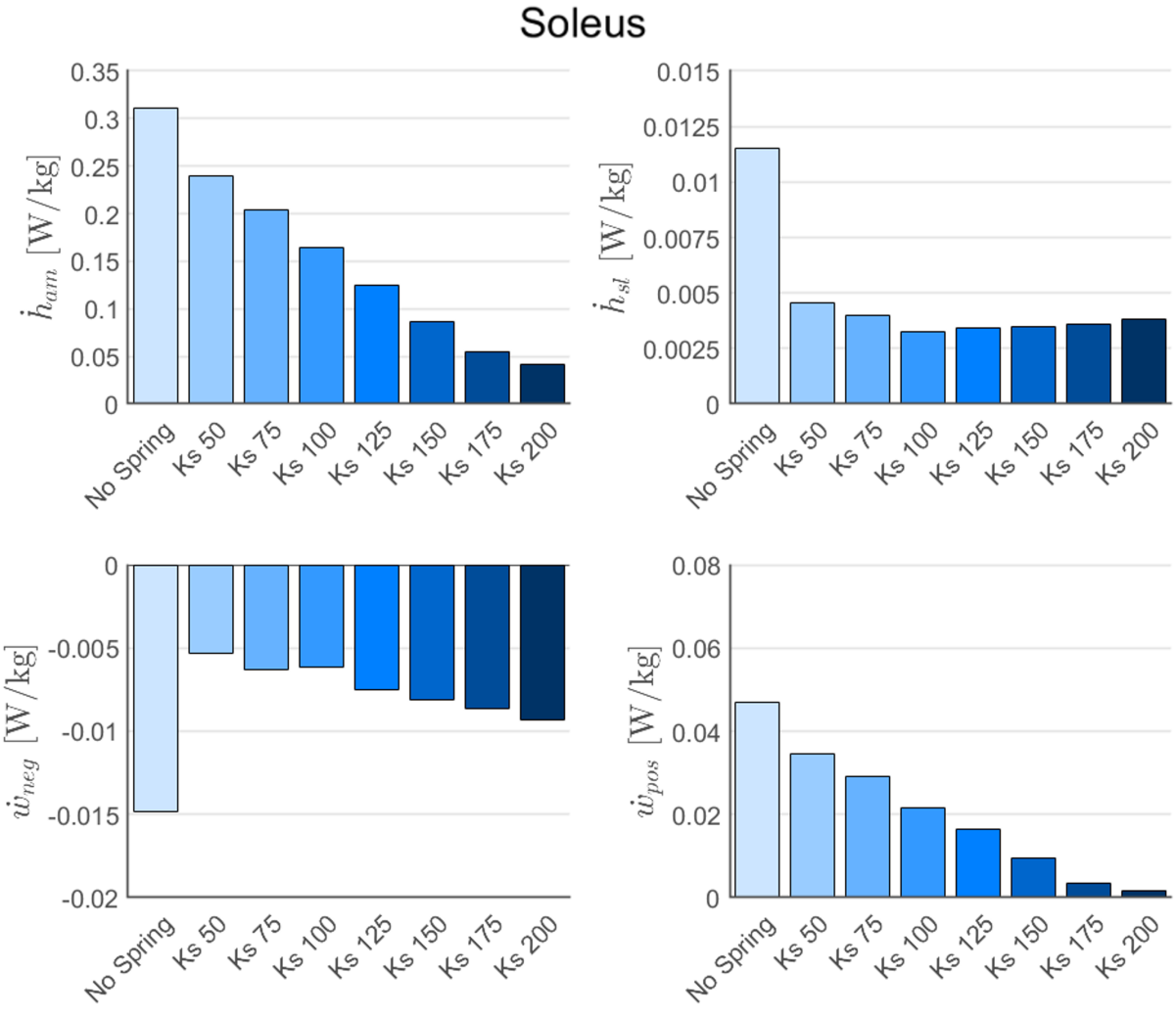

Figure 5.5: Heat and work rates, computed by the muscle energy expenditure model for the soleus, for different K_s values. Top left: activation and maintenance heat rate ($\dot{h}_{am}$); top right: shortening and lengthening heat rate ($\dot{h}_{sl}$); bottom left: negative work rate ($\dot{w}_{neg}$); bottom right: positive work rate ($\dot{w}_{pos}$). Darker blue indicates higher spring stiffness.

The mechanical work rate of the CE, computed through equation 3.12, depends solely on the force

(f^{ce}) and v^{ce}. For analysis, the mechanical work rate was split into negative and positive work rate, since negative work is related to eccentric contraction and positive work to concentric contraction [34]. The increase in average of $\dot{w}_{neg}$ after a certain threshold, while the average of $\dot{w}_{pos}$ continues to decrease, can be explained by the fact that the lengthening velocity average increases more than the shortening velocity's (figure 5.6). Thus, the decrease in force production (figure 5.4b) does not compensate for the increase in velocity, and $\dot{w}_{neg}$ average increases with stiffness after the threshold is reached.

Despite the increase in both $\dot{h}_{sl}$ and $\dot{w}_{neg}$ for stiffnesses over 100 Nm/rad, the total metabolic cost of the stance phase, in what concerns the main agonist decreases steadily with stiffness (figure 5.9). Indeed it seems to decrease more between successive stiffness conditions when stiffnesses are higher than 100 Nm/rad (on average 33%), than when they are lower (on average 20%). This suggests that the decrease in activation and maintenance heat rate and positive work, make up for the imposed changes in muscle mechanics which lead to the increase in shortening and lengthening heat rate and negative work.

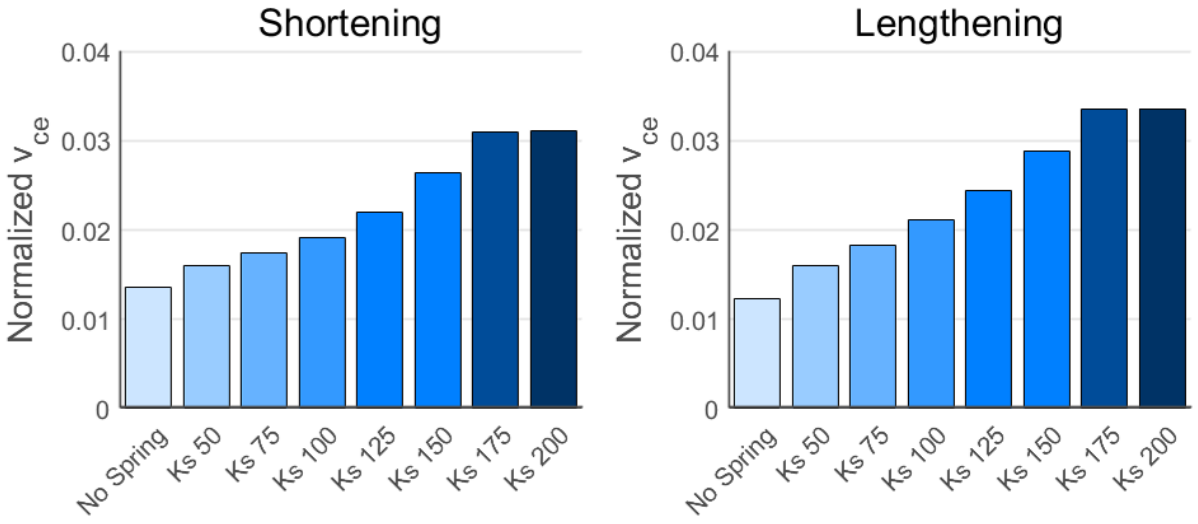

Figure 5.6: Average contractile element velocities: shortening velocity (left); lengthening velocity (right). Darker blue indicates higher spring stiffness.

5.2.2 Tibialis Anterior

The tibialis anterior, after initial contact occurs, acts as an antagonist for the remainder of the stance phase. So, as mentioned in the previous section, it will have to compensate for any excess moment the spring provides. Initially, an increase in spring stiffness requires an increase in force generation by the tibialis anterior at early and late stance, but afterwards, this increase extends to mid-stance (figure 5.7b). Naturally, in order for force production to increase, the muscle's activation must also increase (figure 5.7a). The behaviour of Contractile Element length and tendon length is the opposite of that observed for the soleus, that is, with increasing stiffness l_{ce} decreases while l_{se} increases (figure 5.7cd). For each value of K_s, lengthening velocity peaks at the instant at which the muscle stops producing force during mid-stance (figure 5.7e).

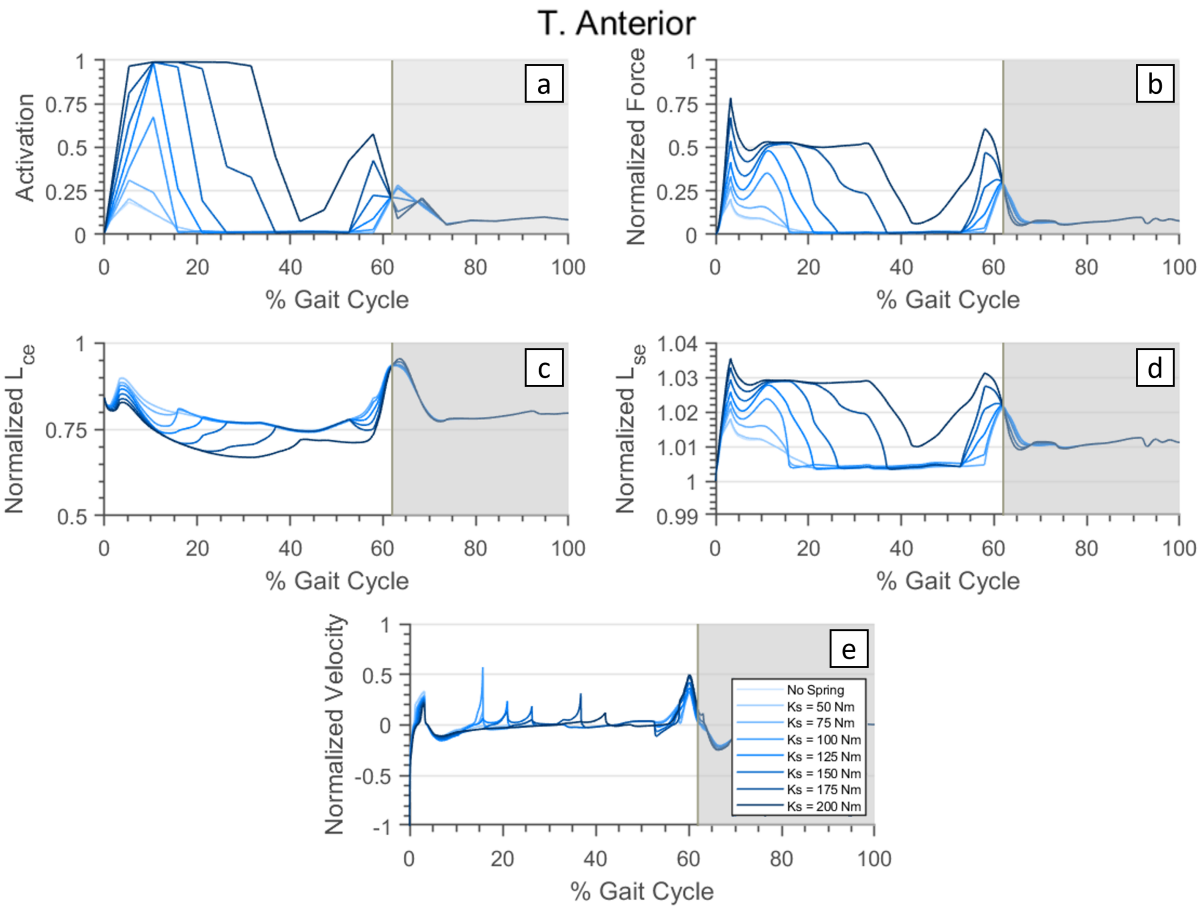

Figure 5.7: Time profiles for the mechanics of the tibialis anterior. Darker blue indicates higher spring stiffness.

This increase, in both activation and force production, leads to the increase in the average of all portions of the muscle energy expenditure rate ($\dot{E}$). For lower stiffness values ($<$ 75 Nm/rad) this increase is extremely small, and then increases substantially once K_s reaches the hundreds (figure 5.8). Once again, by analysing the equations that rule the muscle energy expenditure model, this behavior can be explained. Both heat rates, $\dot{h}_{sl}$ and $\dot{h}_{am}$, are scaled by the activation, while the work rates, both negative and positive, depend on the force produced. In addition to this, $\dot{h}_{sl}$ and $\dot{w}$ also depend on velocity, which does not change much in magnitude, even though the peak lengthening velocity during mid-stance is delayed with increasing stiffness (figure 5.7e). Thus, variations in these portions will mostly be due to changes in activation and force. Both force and activation first increase only during early and late stance, accounting for the small increase in averages obtained for lower stiffness values. For higher stiffnesses, they increase all throughout stance, leading to higher averages of the heat and work rates.

The generalized increase across portions of the muscle energy expenditure rate leads to an increase in the metabolic cost associated with the tibialis anterior during stance (figure 5.9). Initially, for stiffnesses lower than 75 Nm/rad, the increase in metabolic cost between successive stiffness conditions is low (on average 14%), afterwards this increase is significantly higher (on average 41%). This is in line with the fact that, initially, the muscle is only required to produce more moment at early and late stance, and

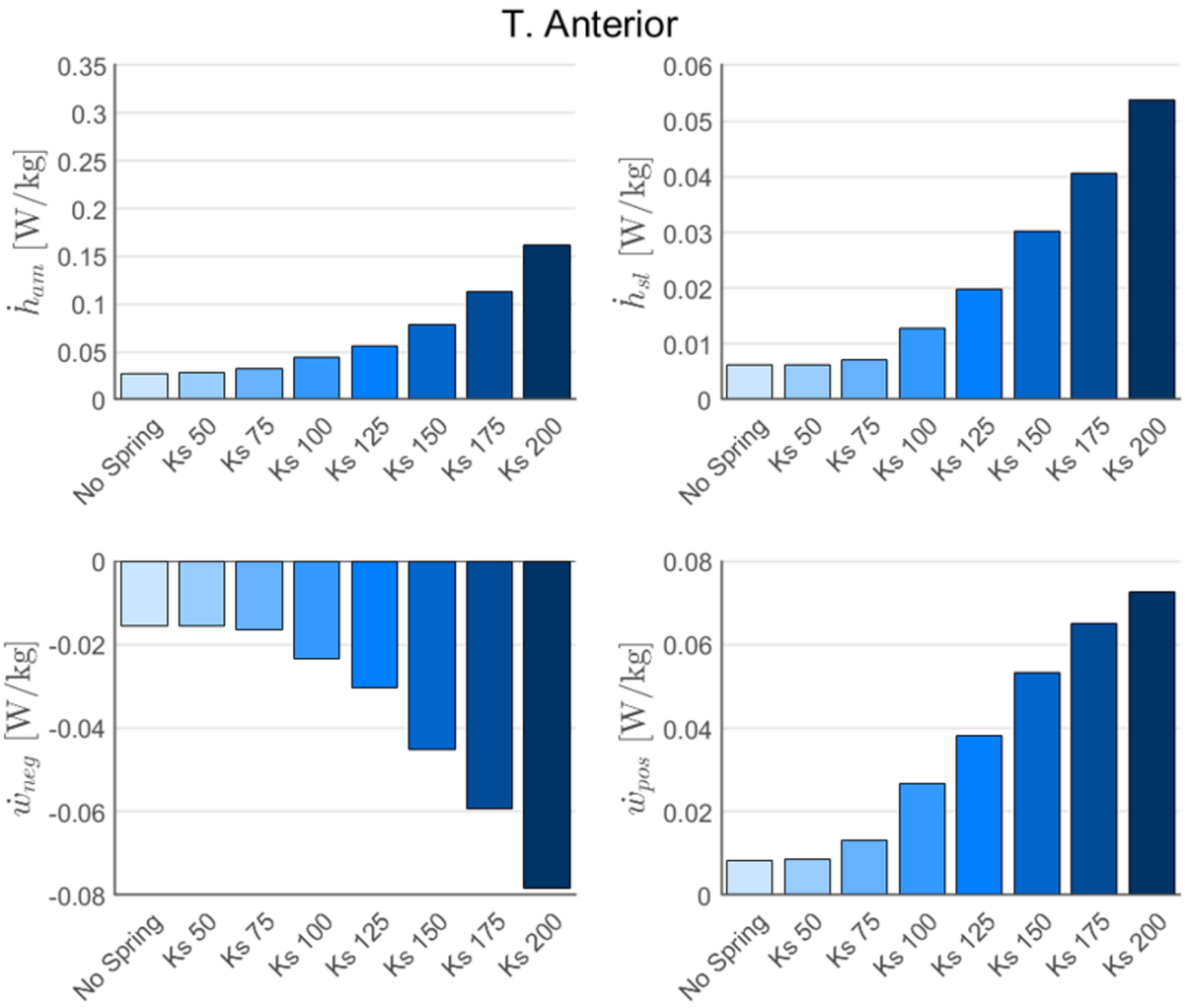

Figure 5.8: Heat and work rates, computed by the muscle energy expenditure model for the tibialis anterior, for different K_s values. Top left: activation and maintenance heat rate ($\dot{h}_{am}$); top right: shortening and lengthening heat rate ($\dot{h}_{sl}$); bottom left: negative work rate ($\dot{w}_{neg}$); bottom right: positive work rate ($\dot{w}_{pos}$). Darker blue indicates higher spring stiffness.

gradually it continues to be recruited throughout mid-stance.

5.2.3 Total Metabolic Cost

The total metabolic cost of the stance phase for the agonist-antagonist pair analysed is simply the sum of the metabolic cost related to each individual muscle (figure 5.9). And while increasing the stiffness of the ankle exoskeleton reduces significantly the metabolic cost associated with the soleus, it also leads to an increase of the metabolic cost associated with the tibialis anterior. Eventually, the increase in metabolic cost associated with the antagonist surpasses the benefit the exoskeleton provides to the agonist. There is, however, an optimal value of K_s for which the metabolic cost of the pair is minimal.

Indeed, for lower stiffnesses, the decrease in metabolic cost associated with the soleus is higher, on average 20% between consecutive K_s values, than the increase of the cost associated with the

tibialis anterior, which is on average 14%. While for higher stiffness values, the opposite is true, a 41% average increase of the metabolic cost associated with the tibialis anterior is observed while the reduction in soleus metabolic cost is on average 33%. The minimum in metabolic cost for the ankle complex musculature corresponds to a stiffness of 150 Nm/rad, which leads to a decrease of 0.1151 J/kg (42.57%) in metabolic cost.

This decrease in metabolic cost is associated with a substantial decrease in the recruitment of the soleus, while the tibialis anterior is developing significantly more force than during unaided stance. This suggests that the soleus is a muscle whose activation and force production is expensive, and that reducing its recruitment, even if it means increasing it elsewhere, will reduce the total metabolic cost of the movement.

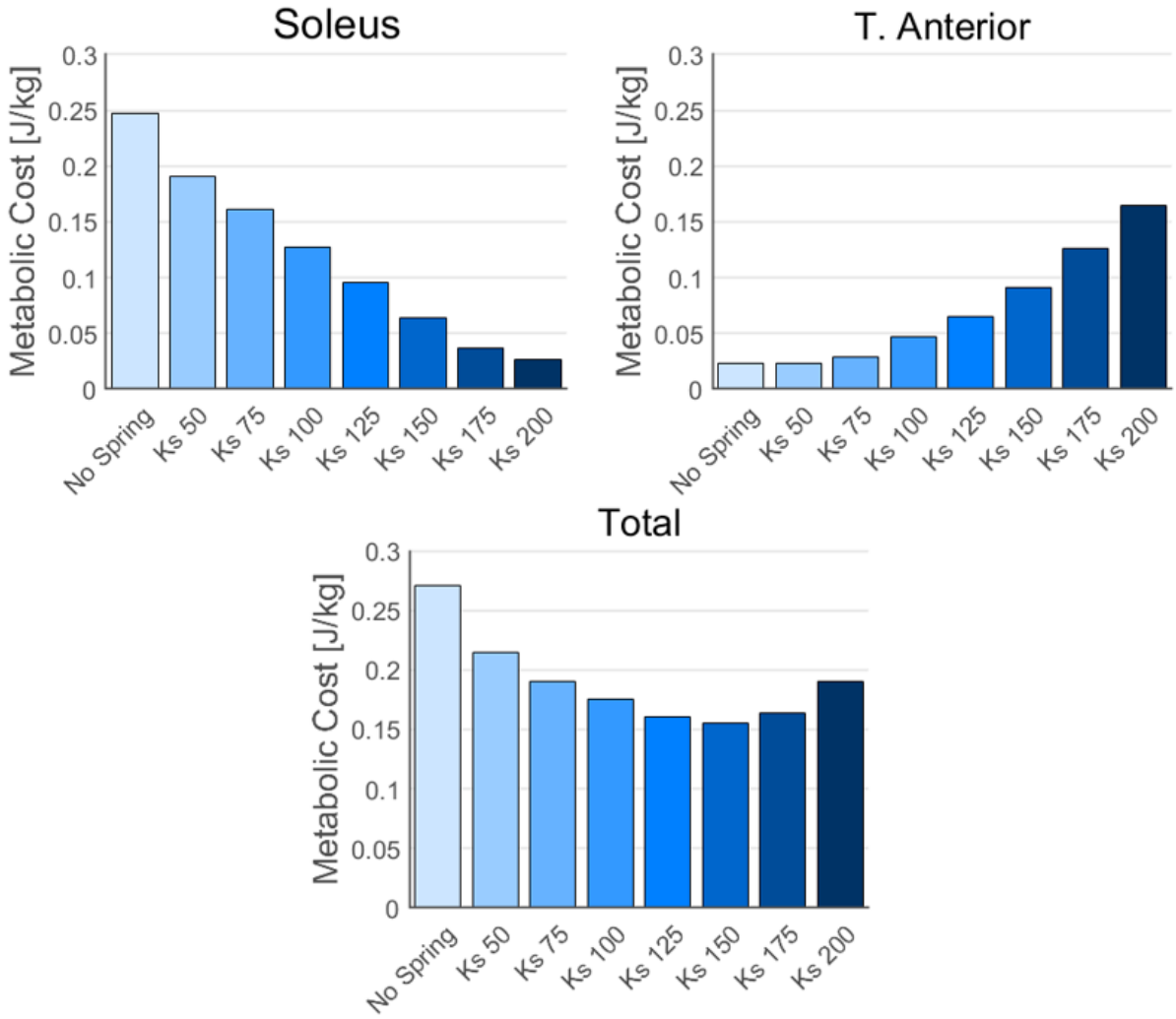

Figure 5.9: Metabolic cost of the stance phase, computed by the muscle energy expenditure model, for different K_s values. On top for both the soleus and tibialis anterior, below the total metabolic cost. Darker blue indicates higher spring stiffness.

5.3 Discussion

The results obtained in this computational analysis support the fact that, adding a parallel stiffness to the ankle joint, will have a beneficial impact on the metabolic cost associated with the joint during walking, at least up to a certain point. This benefit stems from changes in both the mechanics and energetics of the muscles spanning the joint.

The most important of these changes is the reduction in the moment that is required of the plantarflexor, since the parallel spring will generate part of the required moment. This, naturally, reduces the force and activation required of the muscle. As expected, this decrease in force and activation lead to a decrease in metabolic cost associated with the muscle. However, significant changes also occur to the intrinsic mechanics of the soleus muscle-tendon unit, namely the increase in l_{ce} (figure 5.4c) and decrease in l_{se} (figure 5.4d) all throughout controlled dorsiflexion. As explained in section 2.3.3, the MTU is tuned in such a way that, during this stage of the gait, when unaided, the muscle contracts nearly isometrically and the Achilles tendon stretches, accumulating mechanical energy, which it then releases at push off. This is an energetically efficient strategy since the tendon does not require metabolic energy to stretch and recoil, whereas the muscle does require energy for extending and contracting [34]. Thus, adding a parallel spring, which is effectively behaving as a secondary tendon, disturbs these finely tuned mechanics. This effect is noticed particularly on the shortening and lengthening heat rate ($\dot{h}_{sl}$), which increases for higher stiffnesses. Since the muscle is no longer working in its optimal operating range, it will expend more energy for shortening and lengthening its fibers.

Another consequence of the increase in l_{ce} during controlled dorsiflexion is the increase in lengthening velocity, as the muscle must stretch more in the same amount of time, and in shortening velocity, as it will have to contract more at push off. The increase in lengthening velocity is responsible for the increase in negative work rate observed with increasing stiffness. However, as stated before, the increase in shortening velocity does not lead to an increase in positive work rate. When the spring is added to the joint, during controlled dorsiflexion, the muscle is indeed producing more work than before and the tendon is accumulating less energy, while at the same time, the spring is stretching and accumulating the mechanical energy that the tendon would be accumulating otherwise. At push off the muscle contracts faster than it would if unaided, but producing less force, since it is not working in its optimal range and both the tendon and spring recoil, providing the remaining power boost required for PO (figure 2.9c).

The reduction, with increasing stiffness, in metabolic cost associated with the joint is curbed by the fact that, by assuming fixed kinematics, when the moment the spring provides surpasses the physiological moment generated by the soleus, it must be offset by the tibialis anterior. Initially, the tibialis anterior must only compensate for the increase in agonistic moment occurring at early and late stance, but eventually this increase extends to mid-stance. And the benefit experienced by the agonist no longer surpasses the added cost to the antagonist.

This behavior is evident in figure 5.10, where the moment generated by the two muscles being considered is presented, and the straight lines indicate the moment the linear spring generates for a given joint angle, according to equation 4.1. The moment which is above a given straight line, is moment

that still needs to be generated by the soleus, while the moment below the line is negative moment, that must be produced by the antagonist. As spring stiffness increases, the moment above the corresponding line is less, meaning the tibialis anterior is having to generate more moment while the soleus generates less.

It would be expected that a stiffness which generates a moment with a slope parallel to that of the muscle moment vs joint angle curve at the beginning of stance, would provide the most benefit, as it would aid the soleus without requiring further recruitment of the tibialis anterior. Moreover, it is possible to extrapolate that a non-linear stiffness spring would aid the ankle even further, as it would follow the moment vs joint angle curve more closely and provide support to the plantarflexor without disturbing the antagonist. However, this is not the behavior observed, as the tested spring stiffness which most closely reproduces the slope at the beginning of stance phase is 75 Nm/rad, while the greatest decrease in metabolic cost was obtained for a stiffness of 150 Nm/rad. This decrease in metabolic cost is already associated with a significant recruitment of the tibialis anterior. This suggests that the soleus is an expensive muscle to recruit, and so, from an energy saving perspective, reducing the moment required from it, even while increasing the requirement from its antagonist, is beneficial.

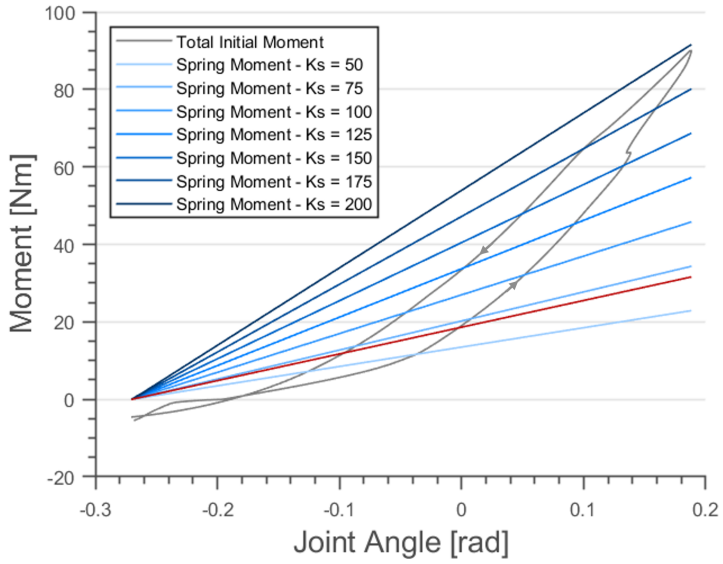

Figure 5.10: Moment vs ankle joint angle curves. In grey total moment of the agonist-antagonist pair before a stiffness is added, in blue the different spring stiffness values tested and in red the slope of the muscle moment vs joint angle curve at the beginning of stance.

The findings in this work match those of Collins et al. [2] who, when measuring the metabolic cost, through indirect calorimetry, of the gait cycle in subjects wearing a passive exoskeleton, obtained a minimum for a stiffness of 180 Nm/rad, corresponding to a decrease in metabolic cost of 7.2%. They identified the increase in tibialis anterior activation as a possible contributing factor for the increase in metabolic cost for the higher stiffnesses tested. As mentioned in section 2.3.3, the effective stiffness of the exoskeleton they developed was around 33% lower than the nominal value. So, in reality the minimum obtained by the researchers corresponds to a stiffness of around 120 Nm/rad, while the next value tested, 240 Nm/rad, actually corresponds to a nominal stiffness of about 160 Nm/rad, already

higher than the stiffness for which the minimum metabolic cost was obtained in this work, which was 150 Nm/rad. The increase in knee muscle activity was another contributing factor identified, but the analysis of the knee joint was not addressed in this project. The other contributing factor identified was the increase in plantarflexor activity at the end of stance. This was not observed with the ankle model developed, because, while the work developed by Collins et al. was based on experimental acquisitions, the work developed for this dissertation was purely computational and considered the kinematics fixed, using the moments generated at the joints during unaided gait to estimate the activations. Therefore, a decrease in moment generated will, most certainly, be tied to a decrease in activation in this model.

The metabolic cost reduction obtained in this work is significantly higher than that obtained by Collins et al., a decrease of 42.57% compared to a decrease of 7.2% obtained by these researchers. This difference is due to the fact that the metabolic cost computed in this analysis only considers the contribution of the soleus and tibialis anterior, while the smaller decrease published by Collins et al. was obtained through indirect calorimetry and thus takes into account the whole body cost.

In their work with the tethered device later developed, Jackson and Collins [33] reached results that diverged from these findings. In their work, an increase of up to 13% in the metabolic cost of walking, estimated by indirect calorimetry, was obtained for a maximum average torque input of 120 Nm to the ankle. However, "effort-related measures at the exoskeleton-side biological ankle" decreased with increasing average torque [33]. Namely, soleus muscle activation was reduced by 24% and total positive ankle work rate decreased by 33%. This is consistent with the findings of this dissertation, for which the soleus activation decreased steadily with increase in stiffness and, up to an added stiffness of 100 Nm/rad the total positive work also decreased. The reasons given for the increase in metabolic cost despite the decrease in effort-related measures at the ankle are cascading whole body effects, and possible changes to the intrinsic mechanics of the plantarflexors.

Further work, using musculoskeletal models, driven by the data acquired experimentally with the tethered device [34] provided insight into the changes suffered by the mechanics of the soleus muscle. An increase in fiber excursion and contraction velocity was found. The same was observed in the analysis with the developed model (figure 5.4ce). Analysis using a muscle expenditure model evidenced a decrease in $\dot{h}_{am}$ and an increase, albeit not very significant, in $\dot{h}_{sl}$, just as in this work. An increase in positive work rate was associated with the increase in fiber excursion and contraction velocity, which was not found through the analysis developed in this work. This difference in behavior is likely due to the fact that the musculoskeletal model, in this dissertation, was driven by data acquired for a computational locomotion model while in the work developed by Jackson et al. [34] it was driven with data obtained for a subject walking with the exoskeleton. Thus, changes caused by the device were all taken into account.

Chapter 6

Conclusions

Human performance augmentation is one of the focuses of exoskeleton development [4]. One of the ways in which human performance augmentation is being pursued is in the reduction of the metabolic cost of human activities, such as gait. Despite being perfected over centuries of human evolution, locomotion still accounts for most of the energy expended during the day [2]. Reducing the cost of this activity could help individuals whose labor is walking intensive to maintain their quality of life for longer as well as to reduce their risk of injury.

A special interested is taken in assisting the ankle joint, since this is the joint which most energy expends during gait. In this dissertation, a computational model of the ankle musculoskeletal complex, comprised of the agonist-antagonist pair soleus - tibialis anterior, was developed. A parallel stiffness was added to the model, making use of a spring, in order to study the effect a passive device would have on the joint. Muscles were modeled as Hill-type muscles coupled to an energy expenditure muscle model. This allowed for the simultaneous analysis of changes to both mechanics and energetics of the muscles when spring stiffness was varied between 0 and 200 Nm/rad.

The analysis conducted using the musculoskeletal model developed, reached results which are congruent with those published by Collins et al. [2], which were obtained experimentally. The developed model estimates the metabolic cost associated with the individual muscles spanning the ankle during stance and allows the analysis of the changes that occur in the mechanics and energetics of the muscles due to the moment being added by the spring. For the data analysed, obtained for the Neuromuscular Locomotion Model [36, 39] walking at 1.3 m/s, a reduction of 42.57% in the metabolic cost associated with the ankle was obtained, when the stiffness added to the joint was 150 Nm/rad.

Provided with experimental acquisitions of the unaided gait cycle, the developed model can be used to estimate the metabolic cost associated with the ankle joint and help select the spring stiffness which would correspond to the greatest reduction in metabolic cost for the individual in question. This is an important contribute to streamlining the fabrication process of the device, since instead of having to test several spring stiffnesses in a laboratory setting, only the acquisition of the natural gait cycle is required to estimate the stiffness best suited to each individual.

6.1 Future Work

During the development of this work opportunities for further improvement and research were identified:

- Addition of the gastrocnemius, part of the triceps surae, to the developed model. This would allow for a more thorough understanding of the changes occurring at the joint level.
- Addition of a muscular fatigue model to the developed implementation in order to study the effect fatigue might have on the behavior observed for the ankle joint when aided by the exoskeleton.
- Acquisition of experimental data with the prototype exoskeleton and using it for driving the developed musculoskeletal model. This would allow for the validation of the results of this dissertation which were based on computational models of human movement.
- Simultaneous acquisition of indirect calorimetry data in order to estimate the total body metabolic cost of the stance phase and thus compare it with the one obtained for the ankle. The order of magnitude of these values is different, but studies have shown there is a correlation [15].
- Performance of the analysis using a non-linear stiffness spring, for instance, a quadratic spring, which more closely follows the behavior of the joint's moment with ankle angle variation during stance. In theory, such a spring would better support the movement and provide a higher reduction in metabolic cost.

References

[1] D. A. Winter. *The Biomechanics and Motor Control of Human Gait*. University of Waterloo Press, Waterloo, 1st edition, 1987.

[2] S. H. Collins, M. Bruce Wiggin, and G. S. Sawicki. Reducing the energy cost of human walking using an unpowered exoskeleton. *Nature*, 522(7555):212–215, 2015.

[3] B. Chen, H. Ma, L. Y. Qin, F. Gao, K. M. Chan, S. W. Law, L. Qin, and W. H. Liao. Recent developments and challenges of lower extremity exoskeletons. *Journal of Orthopaedic Translation*, 5: 26–37, 2016.

[4] L. M. Mooney, E. J. Rouse, and H. M. Herr. Autonomous exoskeleton reduces metabolic cost of human walking during load carriage. *Journal of NeuroEngineering and Rehabilitation*, 7:1–11, 2014.

[5] A. Machado. Concept Development for Lower Limb Exoskeleton. Master's thesis, Instituto Superior Técnico, 2020.

[6] D. Knudson. *The Fundamentals of Biomechanics*. Springer US, Chico, 2nd edition, 2007.

[7] M. W. Whittle. *An Introduction to Gait Analysis*. Elsevier Ltd, 4th edition, 2007.

[8] S. J. Hall. *Basic Biomechanics*. McGraw Hill, 6th edition, 2012.

[9] D. A. Winter. *Biomechanics and Motor Control of Human Movement*. John Wiley & Sons, Waterloo, 4th edition, 2009.

[10] J. Rose and J. Gamble. *Human Walking*. Lippincott Williams & Wilkins, Philadelphia, 3rd edition, 2006.

[11] J. Perry and J. Burnfields. *Gait Analysis - Normal and Pathological Function*. Slack Incorporated, 2nd edition, 2010.

[12] A. M. Dollar and H. Herr. Lower extremity exoskeletons and active orthoses: Challenges and state-of-the-art. *IEEE Transactions on Robotics*, 24(1):144–158, 2008.

[13] T. M. Griffin, T. J. Roberts, and R. Kram. Metabolic cost of generating muscular force in human walking: Insights from load-carrying and speed experiments. *Journal of Applied Physiology*, 95(1): 172–183, 2003.

[14] A. C. Hackney. *Exercise, Sport, and Bioanalytical Chemistry: Principles and Practice*. Elsevier, 1st edition, 2016.

[15] A. D. Koelewijn, D. Heinrich, and A. J. van den Bogert. Metabolic cost calculations of gait using musculoskeletal energy models, a comparison study. *PLoS ONE*, 14(9):1–19, 2019.

[16] R. H. Miller. A comparison of muscle energy models for simulating human walking in three dimensions. *Journal of Biomechanics*, 47(6):1373–1381, 2014.

[17] B. R. Umberger, K. G. Gerritsen, and P. E. Martin. A model of human muscle energy expenditure. *Computer methods in biomechanics and biomedical engineering*, 6(2):99–111, 2003.

[18] A. M. Gonabadi, P. Antonellis, and P. Malcolm. Differences between joint-space and musculoskeletal estimations of metabolic rate time profiles. *PLoS Computational Biology*, 16(10):1–27, 2020.

[19] H. Herr. Exoskeletons and orthoses: Classification, design challenges and future directions. *Journal of NeuroEngineering and Rehabilitation*, 6(1):1–9, 2009.

[20] A. J. Young and D. P. Ferris. State of the art and future directions for lower limb robotic exoskeletons. *IEEE Transactions on Neural Systems and Rehabilitation Engineering*, 25(2):171–182, 2017.

[21] J. A. de la Tejera, R. Bustamante-Bello, R. A. Ramirez-Mendoza, and J. Izquierdo-Reyes. Systematic Review of Exoskeletons towards a General Categorization Model Proposal. *Applied Sciences (Switzerland)*, 11(1):1–25, 2021.

[22] N. O. S&T. Science and Technology Trends 2020-2040. Technical report, NATO, 2020.

[23] A. Zhu, H. Shen, Z. Shen, J. Song, and Y. Tu. Innovative design for portability of unpowered military load exoskeleton robot. *2018 IEEE International Conference on Information and Automation, ICIA 2018*, (2017):744–749, 2018.

[24] B. S. Rupal, S. Rafique, A. Singla, E. Singla, M. Isaksson, and G. S. Virk. Lower-limb exoskeletons: Research trends and regulatory guidelines in medical and non-medical applications. *International Journal of Advanced Robotic Systems*, 14(6):1–27, 2017.

[25] A. Zoss, H. Kazerooni, and A. Chu. On the mechanical design of the Berkeley Lower Extremity Exoskeleton (BLEEX). *2005 IEEE/RSJ International Conference on Intelligent Robots and Systems, IROS*, pages 3465–3472, 2005.

[26] Exoskeleton Technologies: Military. URL `https://www.lockheedmartin.com/en-us/products/exoskeleton-technologies/military.html`. Accessed: 22-03-2021.

[27] M. V. Pillai, L. Van Engelhoven, and H. Kazerooni. Evaluation of a Lower Leg Support Exoskeleton on Floor and Below Hip Height Panel Work. *Human Factors: The Journal of the Human Factors and Ergonomics Society*, 62(3):489–500, 2020.

[28] A. Esquenazi, M. Talaty, A. Packel, and M. Saulino. The Rewalk powered exoskeleton to restore ambulatory function to individuals with thoracic-level motor-complete spinal cord injury. *American Journal of Physical Medicine and Rehabilitation*, 91(11):911–921, 2012.

[29] E. S. Graf, A. De Eyto, M. Sposito, C. Pauli, L. O'Sullivan, C. M. Bauer, E. Bottenberg, D. Scherly, L. Erkens, M. Wirz, J. Ortiz, V. Power, T. Poliero, R. Henke, G. Brinks, and K. S. Stadler. Basic functionality of a prototype wearable assistive soft exoskeleton for people with gait impairments - a case study. *ACM International Conference Proceeding Series*, pages 202–207, 2018.

[30] ReWalk™ Personal 6.0 - ReWalk – More Than Walking. URL `https://rewalk.com/rewalk-personal-3/`. Accessed: 12-03-2021.

[31] M. Bortole, A. Venkatakrishnan, F. Zhu, J. C. Moreno, G. E. Francisco, J. L. Pons, and J. L. Contreras-vidal. The H2 robotic exoskeleton for gait rehabilitation after stroke: early findings from a clinical study. *Journal of NeuroEngineering and Rehabilitation*, pages 1–14, 2015.

[32] R. Rea, C. Beck, R. Rovekamp, M. Diftler, and P. Neuhaus. X1: A robotic exoskeleton for in-space countermeasures and dynamometry. *AIAA SPACE 2013 Conference and Exposition*, pages 1–8, 2013.

[33] R. W. Jackson and S. H. Collins. An experimental comparison of the relative benefits of work and torque assistance in ankle exoskeletons. *Journal of Applied Physiology*, 119(5):541–557, 2015.

[34] R. W. Jackson, C. L. Dembia, S. L. Delp, and S. H. Collins. Muscle-tendon mechanics explain unexpected effects of exoskeleton assistance on metabolic rate during walking. *Journal of Experimental Biology*, 220(11):2082–2095, 2017.

[35] P. Bujalski, J. Martins, and L. Stirling. A Monte Carlo analysis of muscle force estimation sensitivity to muscle-tendon properties using a Hill-based muscle model. *Journal of Biomechanics*, 79:67–77, 2018.

[36] H. Geyer and H. Herr. A Muscle-reflex model that encodes principles of legged mechanics produces human walking dynamics and muscle activities. *IEEE Transactions on Neural Systems and Rehabilitation Engineering*, 18(3):263–273, 2010.

[37] Y. C. Fung. *Biomechanics - Mechanical Properties of Living Tissue*. Springer International Publishing, San Diego, 2nd edition, 1993.

[38] M. Ackermann. *Dynamics and Energetics of Walking with Prostheses*. PhD thesis, University of Stuttgart, 2007.

[39] H. Geyer, A. Seyfarth, and R. Blickhan. Positive force feedback in bouncing gaits? *Proceedings of the Royal Society B: Biological Sciences*, 270(1529):2173–2183, 2003.

[40] B. R. Umberger. Stance and swing phase costs in human walking. *Journal of the Royal Society Interface*, 7(50):1329–1340, 2010.

[41] T. K. Uchida, J. L. Hicks, C. L. Dembia, and S. L. Delp. Stretching your energetic budget: How tendon compliance affects the metabolic cost of running. *PLoS ONE*, 11(3):1–19, 2016.

[42] D. F. Gordon, G. Henderson, and S. Vijayakumar. Effectively quantifying the performance of lower-limb exoskeletons over a range of walking conditions. *Frontiers Robotics AI*, 5(JUN), 2018.

[43] S. Song and H. Geyer. Regulating speed and generating large speed transitions in a neuromuscular human walking model. *Proceedings - IEEE International Conference on Robotics and Automation*, pages 511–516, 2012.

[44] Tutorial (Optimization Toolbox). URL `http://www.ece.northwestern.edu/local-apps/matlabhelp/toolbox/optim/tutori16.html`. Accessed: 03-10-2021.